CERN LIBRARIES, GENEVA

CM-P00062079

AR/Int. SG/65-21
November 29, 1965

ALTERNATIVES TO THE PRESENTLY PROPOSED ISR STRUCTURE

by

K. Johnsen, E. Keil, B. de Raad, L. Resegotti.

The following is a report on investigations of possible magnet structure alternatives for the intersecting storage rings (ISR), including comparisons with the one presented in the "Design Study of Intersecting Storage Rings"[1].

In Chapter I the various structures investigated are listed and discussed briefly. This discussion permits to eliminate most of them on the basis of rather simple arguments.

Chapter II is devoted to the detailed description of a structure which is sufficiently different from the previous one and also sufficiently interesting to warrant serious consideration.

Chapter III describes possible methods of reaching zero degree crossing angles by appropriately distorting the orbits in the two rings.

Chapter IV contains a summary of the advantages and disadvantages of the structures analysed in Chapters II and III with respect to the structure given in [1] and our conclusions.

Finally, an Appendix is added as a digression into the geometry of asymmetrical storage rings with different intersection angles.

---

1) AR/SG Int. 64-9

I. A Discussion of Several Different ISR Structures

I.1. Description of the structures

The study described in this report was initiated in order to investigate the influences of a reduction of the intersection angle and/or an increase of the free space available in the intersection regions on the machine design. The range of intersection angles studied could therefore have an upper limit at the value of 15° which was proposed in [1]. A lower limit is imposed by the finite width of the magnets adjacent to the crossing points. This limit turned out to be in the range $7\text{-}9^\circ$ as the following study indicates.

From the previous design studies it was furthermore known that the number of periods should not be increased much beyond the 48 periods chosen in [1] basically because of the loss of useful space when the circumference is split into shorter and shorter pieces, and because of the increase in gradient. We therefore decided to undertake the present study between 40 and 52 periods. We can then write down the following table which is similar to the Tab. IV.1. in [1].

Table 1. Intersection Angles, Basic Brick and Period Numbers

p/q	ψ	N_1	N_2	M
1/3	15°	16	8	48
2/5	9°	12	8	40
4/11	$12\ 3/11^\circ$	14	8	44
5/12	7.5°	14	10	48
5/13	10.4°	16	10	52

All these structures are very similar in some respects. N_2 only assumes the values 8 and 10. Structures with $N_2 = 8$ can be expected to have more free space in the inner arc than the others. The outer arcs contain 12, 14 or 16 basic building bricks and are also more closely packed when N_1 is high.

It can be deduced from the table above that the structure with 52 periods is the worst of all possible choices because it has the highest number of periods both in the inner and the outer arcs. Therefore we must expect that it is about as crammed as a 15° structure in the outer arc, and as crammed as a 7.5° structure in the inner arc. For this reason we eliminate it from further investigation already at this stage.

The main parameters of the remaining structures are given in Tab. 2. The quantities entering into it are self-explanatory. The interaction rate is proportional to $\left[\sqrt{\beta_{VIR}}\tan(\psi/2)\right]^{-1}$.

Structure no. 1 is the one adopted by the Study Group half a year ago. It is a slightly modified version of the structure presented in [1). Its intersection region geometry is identical to that of [1), but the lengths of a_4 and a_6 are slightly changed. This yields a small reduction in aperture requirements, and makes the parameters of this structure slightly different from those given in Tab. IV.3. of [1).

Structure no. 2 has resulted from the analysis of the implications of asking for 20 m free space in the interaction region in a 15° structure. The only practical method of achieving this would be to reduce the length of the magnet units slightly which necessarily means a reduction in the design energy to 26.6 GeV. The resulting structure turned out either to require a very difficult injection or a very large vertical aperture and it was therefore dropped. However, the compromise structure no. 2 in the table was found to be worth further considerations. It was arrived at by keeping the reduced energy (26.6 GeV) and reducing the free space in the interaction region by one metre in order to gain 2 m in the middle of the inner arc for the injection septum magnet. A variant of structure no. 2 would be one still having 28 GeV design energy but with its average radius increased by 5 m. Because of the given size and shape of the ISR site we do not consider this a practical proposal.

In structure no. 3 a crossing angle of 7.5° is achieved by transferring four of the 48 periods from the outer into the inner arcs. Correspondingly, the free space in there becomes rather limited. In fact most of the correction equipment would have to be removed from the inner arc in order to leave space free for the equipment for injection which just seems possible when the parameters of all the components are pushed. Additional mid-F and mid-D straight sections for correction equipment must therefore be provided in the outer arcs.

Structure no. 4 is an example of a structure with 40 periods and 9° crossing angle. Due to the reduced number of periods it can be built with short magnets in a FOFDOD arrangement if one makes the gap between unlike magnets just long enough for the coil overhangs and a vacuum chamber connection. Since this structure has the same number of periods (i.e. 4) in the inner arcs as a 15° structure, and since there are only small gaps between unlike magnets, the long mid-F straight sections are almost as long as in the 15° structure although the magnets and the intersection regions are longer. The lengths of a_4 and a_6 are chosen such that the maximum vertical β-value is as small as possible. A variant of this structure is one where the magnets are arranged in a FODO fashion. Because of the smaller flexibility of the FODO arrangement and because of the shorter mid-F straight sections we consider it less attractive than the FOFDOD structure given.

Structure no. 5 is a structure with 44 periods and $12\ 3/11^{\circ}$ crossing angle. Since it has one period more in the outer arc than a 9° structure there is not enough space to split long magnet units into two short ones. As a consequence the magnet lattice must be FODO. The useful free space available in the inner arcs is shorter than in the 15° structure since the magnets and the intersection regions are longer; it is also shorter than in structure no. 4 because of the straight sections inserted between unlike magnets.

Structure no. 6 is an asymmetric structure with two different crossing angles. A more detailed evaluation of designs with unequal intersection angles will be given in an Appendix.

Table 2. Parameter List for ISR Structures

Structure		1	2 x)	3	4	5	6	
Number of periods	M	48	48	48	40	44	48	
Periods in outer arc	M_1	8	8	7	6	7	7	
Periods in inner arc	M_2	4	4	5	4	4	5	
Intersection angle	ψ	15°	15°	7.5°	9°	$12\ 3/11^\circ$	7.5°	av.
Magnet unit length	L_u	2.44	2.32	2.44	2.95	2.70	2.44	m
F-D straight section	a_o	1.63	1.63	1.63	0.88	1.63	1.63	m
D-D, F-F " "	a_1	0.15	0.15	0.15	1.63	0.15	0.15	m
Interaction region	a_2	16.78	18.71	19.5	20.0	20.0	16.13 / 30.73	m
Straight section	b_1	6.98	9.01	9.22	10.13	9.90	6.00 / 20.60	m
" "	b_2	9.80	9.70	10.28	9.87	10.10	10.13	m
" "	a_3	1.0	2.0	2.0	1.63	2.0	2.0	m
" "	a_4	13.08	14.03	8.26	12.14	12.93	7.26	m
" "	a_5	3.0	2.0	1.0	2.5	2.0	2.0	m
" "	a_6	9.40	9.50	1.8	9.55	5.24	1.8	m
" "	a_7	-	-	4.59	-	-	4.45	m
Profile parameter F	$(n/\rho)_F$	-3.14	-3.19	-3.23	-3.08	-2.95	-3.26	m^{-1}
" " D	$(n/\rho)_D$	+3.05	+3.10	+3.18	+2.99	+2.85	+3.21	m^{-1}
	$\beta_{H\ max}$	37.9	41.9	48.6	39.4	37.3	50.3	m
	$\beta_{V\ max}$	50.2	54.4	70.9	65.0	62.4	98.2	m
	β_{VIR}	13.0	14.5	24.0	22.9	18.3	30.5 / 30.7	m
	$\alpha_p(F)$	2.27	2.23	2.28	2.34	2.30	2.28	m
	$\alpha_p(D)$	1.52	1.50	1.52	1.51	1.49	1.51	m
Vertical aperture		49	53	64	57	58	88	mm
Horizontal aperture		142	146	154	141	142	158	mm
$(\sqrt{\beta_{VIR}}\ \tan\psi/2)^{-1}$		2.12	2.00	3.12	2.67	2.19		
Maximum radius R_{max}		154.4	154.6	152.6	153.3	154.1		m
Minimum radius R_{min}		145.3	145.2	148.3	147.1	146.3		m
Interaction radius R_{int}		148.6	148.3	148.5	148.7	148.4		m

x) This structure gives only 26.6 GeV total energy in each ring.

We believe that this list of ISR structures includes all possible structures with fundamental design differences. There is, of course, an infinite number of variations to these structures but their properties are probably close to, and in most cases inferior to, those of the structures given above. This is due to the optimization of the layout done wherever possible.

I.2. Arguments for the selection of ISR structures

The following features should be considered in a comparison of various ISR structures:

i) general machine layout and engineering
ii) betatron oscillation amplitudes, momentum compaction factors
iii) aperture requirements
iv) injection possibilities
v) ejection possibilities
vi) possibilities for physics experiments
  a) space around the interaction regions
  b) interaction rate
vii) possibilities for head-on collisions
viii) cost
ix) the time delay in the construction programme.

I.3. First elimination of a few structures

The list of structures given in Table 2 is too long for all of them to be investigated in great detail within a short time. This is, however, not necessary since some of them can be eliminated on the basis of the data contained in Table 2.

In the elimination process we shall mostly compare the structures in pairs and only consider the better structure from there on.

The lengths of the intersection regions being equal - the 1.5° difference in crossing angle of 9° and 7.5° structures and the even smaller relative difference in interaction rate are not important arguments in a choice between them from an experimental physics point of view. The advantages of the small gain in interaction rate may even be smaller than the disadvantages from the reduced accessibility of the intersection regions due to the fact that the magnets of outer and inner arc are almost touching each other in a 7.5° structure. We conclude that there are no important physics arguments in the choice between the two kinds of structures.

The machine design arguments are all in favour of a 9° structure. 7.5° structures need very difficult injection schemes, a much bigger aperture and therefore bigger and more expensive magnets. This is quite in contrast to 9° structures which have enough space to allow short magnet units (and thus only one type of F and D magnets), are less difficult to inject into and need less increase in aperture. We therefore eliminate the structure no. 3 from further considerations.

Difficult injection and considerably higher aperture are also features of the asymmetrical structure no. 6. Since the general layout of structures with unequal crossing angles is different from that of symmetrical structures we give a brief discussion of the geometry and of the resulting orbit parameters of such structures in an Appendix. We may summarize the result of this evaluation by saying that we have not found that asymmetrical structures present advantages that could outweigh the technical disadvantages.

Let us then compare structure 5 with 4 and 1 (or 2). If one attaches much importance to a small crossing angle the step from 15° to $12\ 3/11^{\circ}$ seems small and one should go to 9°, which also would give $25^{\circ}/o$ larger interaction rate. If long straight sections are very important one finds this advantage also in 2, and with only marginally smaller interaction rate. From a machine point of view no. 5 is clearly inferior both to 4 and 1 (or 2). For instance, injection is easier in both 4 and 1, and the magnets are smaller. For these reasons we do not present more details on structure 5 in this report.

After this elimination process we are left with structures

1, 2, 4

We consider structure no. 1 adequately discussed by referring to the structure represented in[1] of which it is a small modification. We also consider structure no. 2 to be sufficiently similar to structure 1 not to require a special description in addition to the data given in Table 2.

In the following chapter more details are given on the 9^{o} FOFDOD structure no. 4 in order to make possible a detailed comparison with the other two structures.

II. Description of the 9^{o} FOFDOD Structure

II.1. Layout of the structure

The structure has 40 periods, thus 10 periods in a superperiod. They consist of 5 compact periods, forming the central part of the outer arc, and 5 expanded periods arranged such that the intersections take place near the centres of the two extreme expanded periods. The layout of one octant of this machine is shown in Fig. 1, the whole machine is shown in Fig. 2.

The average radius of the ISR is 150 m. The average radius of the compact lattice is 107.0 m, and that of the expanded lattice is 193.0 m, the intersection points are on a circle of 148.7 m radius.

The long straight sections are all mid-F since this is necessary for the intersection regions and for injection and ejection purposes, in particular for the fast kicker magnets associated with them. The interaction rate is inversely proportional to the beam height which has relative minima in mid-F. The distance between the injection kicker and the edge of the stack is fixed by the condition that the kicker stray field must not disturb the stacked beam. Therefore the kicker magnet(s) should be in azimuthal positions where the momentum range covered by this distance is a minimum. This is also achieved in mid-F.

From this point of view the mid-D straight sections in the inner arc need not be longer than those in the outer arc. This is even advantageous since it yields the longest mid-F straight sections. However, we have tentatively made two of them about 0.8 m longer in order to provide more space for sextupoles and other correction equipment which are to be used together with corresponding equipment in the long mid-F straight sections.

For fixed lengths of the interaction regions and of the mid-D straight sections the remaining mid-F straight sections were chosen such as to minimize the maximum value of the vertical β-function. The resulting variation of the horizontal and vertical β-functions along half a superperiod is shown in Fig. 3. Because of the choice of a_4 and a_6 the two highest peaks of the vertical β-function are equal. For other choices of a_4 and a_6 one of them would be higher than shown in Fig. 3, and the other one lower.

II.2. Magnetic field and gradient

The average length of the magnet units is fixed by choosing the maximum field on the equilibrium orbit and the maximum total energy of the protons which should be approximately equal to the maximum energy available from the CPS, namely 28 GeV.

For the reasons given in [1] we choose a maximum field on the equilibrium orbit of approximately 1.2 T. The bending radius is then 79.2 m and, if there are four magnet units in a period, the length of a unit is $L_u = 2.95$ m.

The information gathered so far can be used to compute the magnetic field gradient if we neglect fringe field effects for focusing for the time being; the result is

$$\begin{aligned}(n/\rho)_F &= -\,3.08\ \mathrm{m}^{-1}\\ (n/\rho)_D &= +\,2.99\ \mathrm{m}^{-1}\end{aligned} \qquad (1)$$

The actual profile parameters with the fringe field effects for focusing taken into account will be lower than the ones given in (1) since the focusing length of the magnet units is longer than the core length L_u used.

II.3. Aperture requirements

In the following section we make the same assumptions as in IV.6. of [1]. We thus can limit the discussion to a pure listing of the new figures.

II.3.1. Beam emittance

Scaling beam radii with $\sqrt{\beta_{max}}$ yields at 25 GeV.

$$\hat{x} = 4.7 \text{ mm and } \hat{z} = 6.0 \text{ mm} \tag{2}$$

II.3.2. Injection space and errors

We scale injection errors as β_{max} and obtain

$$\begin{aligned} \hat{x}_{inj} &= 5.9 \text{ mm} \\ \hat{z}_{inj} &= 5.0 \text{ mm} \end{aligned} \tag{3}$$

Combining (2) and (3) gives the following figures for the maximum width w and the maximum height h of the beam at 25 GeV:

$$w = 21.2 \text{ mm and } h = 22.1 \text{ mm} \tag{4}$$

whereas the beam height in the intersection regions becomes

$$h_{IR} = 13.1 \text{ mm} \tag{5}$$

We also assume that a distance of 36 mm is necessary between the injection orbit and the edge of the stack in order to avoid that the kicker stray field affects the stacked beam.

II.3.3. Influence of random magnet errors

For the computation of closed orbit distortions we follow the procedure outlined in IV.4.4.2. of [1]. From the behaviour of the β-functions plotted in Fig. 3 we deduce that

$$\beta_{av} = 1/2\ \beta_{max} \tag{6}$$

and obtain for closed orbit responses to misalignments

$$\begin{aligned} X_{98}(\delta) &= 42\ \delta \\ Z_{98}(\delta) &= 69\ \delta \end{aligned} \tag{7}$$

and to magnetic field errors

$$X_{98}\ (\delta B) = 14\ \delta B/B \tag{8}$$

We assume the r.m.s. magnet imperfections given in Tab. IV.9 of [1] and obtain the following values of the closed orbit distortions which will not be exceeded in 98°/o of all machines:

$$\begin{aligned} X_{98}\ (\text{total}) &= 12.5\ \text{mm} \\ Z_{98}\ (\text{total}) &= 12.0\ \text{mm} \end{aligned} \tag{9}$$

II.3.4. Aperture for stacking

The design momentum spread in the stack is $\delta p/p = 2.5°/o$. The maximum momentum compaction function can be taken from Table 2 and this gives the maximum width of the stack as $\delta x = \alpha_p\ (\text{max})\ \delta p/p = 59$ mm.

II.3.5. Vertical aperture for multiple scattering

Assuming the same relative amplitude increase due to multiple scattering as in [1], we obtain a vertical aperture for the beam of 33 mm at 25 GeV.

II.3.6. Conclusions for the aperture

In the following we combine the figures obtained in the preceeding sections to determine the aperture required. They are based on the beam characteristics at 25 GeV.

The horizontal aperture is made up as follows:

Stack width	59 mm
Distance from the injection orbit to the edge of the stack	36 mm
Beam size	21 mm
Closed orbit distortions	25 mm
	141 mm

The vertical aperture is given by the following two contributions:

Beam size including gas scattering	33 mm
Closed orbit distortions	24 mm
	57 mm

II.4. Arrangement of auxiliary equipment

The number of straight sections long enough for putting in auxiliary equipment like electrostatic pick-up stations and correcting magnets is 33 in a superperiod of the 15^{o} structure[1]. In the 9^{o} FOFDOD structure there are only 20 straight sections available because of the smaller number of periods (and magnets) and because of the FOFDOD arrangement. Therefore the amount of auxiliary equipment has to be reduced and some of the straight sections have to be chosen such as to provide room for more than one piece of equipment simultaneously.

A tentative distribution of the straight section space is given in Fig. 2. The following equipment is foreseen in each ring:

a) 44 electrostatic pick-up stations; they are distributed such that the maximum phase advance between neighbouring stations is about 0.3 wavelengths. Eight of them must be inside radial field magnets and therefore may be of inferior quality than the others.

b) 16 Terwilliger quadrupoles, 8 horizontally focusing ones in the interaction regions and 8 vertically focusing ones in the centres of the inner and outer arcs.
c) 16 radial field magnets arranged about one quarter betatron wavelengths before and after each intersection region for vertical beam position adjustment at the crossing points.
d) 32 quadrupoles with their axes at 45° (skew quadrupoles) for decoupling horizontal and vertical betatron oscillations.
e) 16 sextupoles in four of the straight sections of each inner arc for changing the dependence of the Q-values on momentum.

II.5. Superposition of closed orbits

A small beam width in the intersection regions, which is desirable for certain types of experiments, and - under certain conditions to be discussed below - for increasing the interaction rate when used together with head-on collisions, can be obtained by superposition of the closed orbits for different momenta there. Terwilliger[2)] has shown that this can be achieved by applying a harmonic gradient perturbation to the magnet structure with a harmonic number close to Q.

In Fig. 4 a distribution of Terwilliger quadrupoles is given together with the momentum compaction function $\alpha_p(s)$ over a superperiod. In this symmetrical arrangement of the Terwilliger quadrupoles all closed orbits are made coincident at all intersection points with an angle of about 1 mrad between the extreme closed orbits for a stack width $\Delta p/p = 2.5\,^{o}/o$. This angle is of the same order of magnitude as the angle due to betatron oscillations and injection errors. A total number of 16 quadrupoles is used with the following strengths:

$$8 \text{ F quadrupoles with } C = -0.0096 \text{ m}^{-1}$$
$$8 \text{ D quadrupoles with } C = +0.0096 \text{ m}^{-1}$$

The Terwilliger scheme has the following effects on the orbit parameters and machine performance:

The ratio between the maximum momentum compaction function with and without Terwilliger quadrupoles excited is 2.14. Since the

2) K.M. Terwilliger, Proc.Int.Conf. High En. Acc. CERN, p. 53 (1959).

PS/5136

maximum beam intensity is proportional to the ratio of stack width to maximum momentum compaction it will be reduced when the Terwilliger scheme is applied. The exact amount of the remaining intensity depends on the operation of the scheme and will be discussed in II.6.

This scheme leads to a 15°/o increase in the maximum value of the vertical β-function.

When the beams collide with zero crossing angle in the schemes to be discussed in chapter III, an increase of the interaction rate is possible due to the reduction of beam width brought about by using the Terwilliger scheme. However, one must distinguish between several distinct cases in the combined application of head-on collisions and Terwilliger scheme.

Obviously, the reduction in beam width is most pronounced for the widest possible stack. But the corresponding increase in interaction rate could only be obtained in a storage ring with an increased horizontal aperture. In all cases where the width of the stack is limited by the available horizontal aperture, the gain in interaction rate due to the smaller beam width is compensated by the reduction in the intensity of both beams. Therefore the application of the Terwilliger scheme together with head-on collision will not increase the maximum achievable interaction rate significantly, as will be shown in III.5.

With decreasing momentum spread one will reach a point where the beam will just fit into the aperture with the Terwilliger quadrupoles excited. This occurs at about 1-1.5°/o momentum spread, and then one can get the full gain from the reduction in the width of the beam. This will be a factor 2 to 3.

For considerably smaller momentum spread the width of the beam will predominantly be determined by the betatron oscillations amplitude, and the application of the Terwilliger scheme will have practically no effect on the interaction rate.

II.6. Beam transfer

II.6.1. Design of the injection system

The injector components are located in the long mid-F straight sections a_4 and a_6 of the inner arc. The beam to be injected approaches the vacuum chamber at a fairly large angle in a long mid-F straight section. It is made parallel to the central orbit by a septum magnet and then deflected onto the injection orbit by a fast kicker magnet in the next mid-F straight section. We prefer to inject from the inside in a long mid-F straight section because the beam then enters the machine on the open side of the magnet pole where the aberrations are much smaller than on the closed side. Since the CPS is about 10 m lower than the ISR the beam is brought to the inside of the ISR by passing under the magnet units. Over the last part of its trajectory it rises with a slope of about 10 $^{o}/o$ and is finally deflected horizontally and vertically until it is parallel to the central orbit. This is shown schematically in Fig. 5.

II.6.2. Optimum injector position

There are two possibilities for locating the injection equipment after the decision on injection in a long mid-F straight section is taken:

i) the septum magnet is in an upstream a_4 and the kicker in the a_6 straight section

ii) the septum magnet is in a_6 and the kicker in the downstream a_4 straight section.

The following arguments enter into the choice:

i) The lengths available in the straight sections a_4 and a_6. They are given in Table 3.

ii) The values of the β functions there, also given in Tab. 3.

iii) The width of the stack when the Terwilliger scheme described in II.5. is used.

iv) The distance of the injection trajectory from the next upstream intersection region.

Let A be the maximum stack width, excluding betatron oscillations, that can be allowed at any azimuth during stacking, and B the distance from the injection orbit to the bottom of the stack. $\alpha_p(F)$ is the unperturbed value of the momentum compaction function in mid-F, $\alpha_p(K)$ and $\alpha_p(max)$ are its values at the kicker and the maximum respectively when the Terwilliger quadrupoles are excited. If they are turned on after the stacking is finished one can also use part "B" of the aperture to accommodate the stack. In this case the ratio between the maximum stacked currents with and without Terwilliger scheme is

$$R_1 = \frac{A + B}{A} \; \frac{\alpha_p(F)}{\alpha_p(max)} \tag{10}$$

If one decides to stack with the Terwilliger quadrupoles excited, e.g. because of a special small vacuum chamber in an intersection region, the maximum stacked current is reduced by the factor

$$R_2 = \left[1 - \left(\frac{\alpha_p(max)}{\alpha_p(K)} - 1\right)\frac{B}{A}\right] \frac{\alpha_p(F)}{\alpha_p(max)} \tag{11}$$

It is clear from eq. (11) that the largest value of R_2 is obtained if the kicker is at such a place that $\alpha_p(K) = \alpha_p(max)$. The quantities entering into eq. (10) and (11) and the resulting values of R_1 and R_2 computed with the assumptions A = 59 mm and B = 36 mm are included in Tab. 3.

Table 3. Parameters related to the injection kicker position

Kicker position	a_4	a_6	
Total straight section length	12.14	9.56	m
Horizontal β value	25.5	26.5	m
Vertical β value	9	24.5	m
$\alpha_p(F)$	2.34	2.34	m
α_p (max)	5.01	5.01	m
$\alpha_p(K)$	3.25	4.73	m
R_1	0.76	0.76	
R_2	0.31	0.46	
Horizontal distance of injection orbit from the upstream crossing point	8	1.6	m
Vertical distance of injection orbit from the upstream crossing point	4.5	1.6	m

II.6.3. Choice of the injector position

Two of the arguments presented in II.6.2. are in favour of locating the kicker magnet in a_6 and two are in favour of putting it into a_4.

i) If the kicker is in a_6, the septum magnet , which needs more space than the kicker can be in a_4, which is longer than a_6. This argument is, however, not very strong since the studies carried out on structure 1 have shown, that a straight section of 9.4 m length, with also a Terwilliger quadrupole present, is just sufficient to allow injection from the inside.

ii) The reduction in maximum stacked current with the Terwilliger quadrupoles excited during injection is less drastic when the kicker magnet is in a_6. The difference between the two schemes is, however, relatively small.

iii) If the kicker magnet is in a_6, its gap height must be 1.65 times larger than in a_4.

...) If the kicker magnet is in a_6 the injection trajectories are so near to the next upstream intersection regions that they are practically lost for experiments.

We have decided to put the septum magnet into a_6 and the kicker into downstream a_4, mainly because of iv), since we consider blocking two intersection regions right from the beginning a very serious decision which should only be taken if there were strong reasons for doing so.

II.6.4. Beam dumping and ejection

We have also studied beam dumping and slow ejection but we shall make only a few comments about them.

The small value of the vertical β function in a_4 makes this a very attractive place for various special magnets, e.g. for beam dumping. One could locate two bump magnets in the upstream and downstream a_4 straight sections half a wavelength apart. By pulsing them simultaneously from a capacitor bank one could drive the beam into a dump target in a_6 without perturbing the closed orbit in the rest of the machine.

For slow ejection at Q = 9 a special ejection quadrupole could be put into downstream a_4. It would increase the vertical betatron amplitude by about 20 °/o which is less than the allowance for multiple scattering.

III. Special Magnets for Experiments and Head-On Collisions

1. Special magnet sections for small angle scattering

For the study of elastic or nearly elastic scattering at small (say 50 mrad) angles a good momentum resolution is required, but it is difficult to place analyzing magnets close enough to the ISR magnets. Therefore it may be desirable to extend some of the ISR magnet units radially, so that their field can also be used to analyse the scattered protons. This procedure is difficult with strong focusing magnets and in such cases it looks preferable to replace the first F and D magnet units downstream of the crossing point by a large homogeneous field magnet with a quadrupole with open median plane at each end. To cover an angular range of e.g. 50 mrad at 12 m. from the crossing point, the good field region of the large magnet should extend over about 600 mm from the orbit on the side of interest. Its gap height could e.g. be 200 mm and its maximum field 1.5 T. A possible layout for the structures 1 and 4 is shown in Fig. 6. In structure 4 the separation of the orbits in the two rings at 11 m from the crossing point is about 1.7 m and from the diagram one sees, that this is just enough for the special magnets mentioned above. In front of magnet M' there is only limited space for access to the open side of the gap and both the yoke of M and M' must be on the inside of the equilibrium orbit. In structure 1 there is enough space to place the yoke of M on the outside of the equilibrium orbit or alternatively to use even larger special magnets if the need for them would arise. Each of the special magnets shown in Fig. 6 would have a weight of about 250 tons in structure 1 and 300 tons in structure 4. The difference is due to the difference in length of the magnet periods in the two machines. The longer magnet of machine 4 gives a correspondingly higher momentum selection.

2. Magnet strengths for head-on collisions

It has been suggested that for certain experiments it would be advantageous, if the crossing angle ψ could be made much smaller (say 1° or 2°) or if the beams could be made to collide head-on. Two possible methods to achieve this are shown schematically in Figs. 7a and 7b. In Fig. 7a all bending magnets are located in the crossing straight section a_2. The sum of the deflection angles for each bean is then about 2.5 ψ. An important reduction in magnet strength can be obtained by placing a bending magnet M_3 in the adjacent straight section a_4 of the inner arc. The distance between M_2 and M_3 is about 30 m. As shown in Fig. 7b the ISR magnet period between M_2 and M_3 must then be displaced laterally over a distance of about 0.6 m to 1.5 m depending on the type of machine and the particular arrangement chosen. Table 4 gives the bending magnet strength that is required to obtain head-on collisions at 28 GeV.

Table 2. Values of $\int Bdl$ for head-on collisions

		$\int Bdl$ per beam in a_2	Total $\int Bdl$ of all special magnets
all magnets in a_2	$\psi = 15^{\circ}$	52 Tm	80 Tm
	$\psi = 9^{\circ}$	35 "	45 "
magnets in a_2 and a_4	$\psi = 15^{\circ}$	28 "	40 "
	$\psi = 9^{\circ}$	16 "	22 "

Broadly speaking we can subdivide the 4 cases listed in the Table into the following three categories.

With all magnets in a_2 and $\psi = 15^{\circ}$ (i.e. structures 1 and 2 in Table 2) we need magnetic fields of 8-10 T. This is somewhat beyond what is feasible with present superconducting materials. Even if better materials are developed, the enormous magnetic forces and large stray fields will present difficult engineering problems. If solutions to these problems could be found they are likely to be expensive and therefore we shall not consider this case any further.

The two following lines in Table 4 require magnets with a field of about 4 T. Such fields have already been reached at present in magnets with dimensions of the order of 1 m so that these two cases look realistic. We shall therefore base the further analysis on superconducting magnets with a field of 4 T.

With magnets in a_2 and a_4 in the 9^o machine the values of $\int Bdl$ are sufficiently low, that one can even obtain head-on collisions with conventional steel magnets with fields in the range 1.5 T to 2.0 T. One might, of course, prefer to use also in this case superconducting magnets, which can then be correspondingly shorter.

3. Some remarks about superconducting magnets

Although this matter has not been studied adequately in the limited time available for this study it is nevertheless useful to make a few elementary comments on those aspects of superconducting magnets that are relevant for this discussion. Let us start by considering the required field homogeneity. If the total bending magnet length in a_2 is 8 m, and the gradient $\partial B_x/\partial z$ at the beam position, due to field inhomogeneity is 10 gauss/cm, the amplitude of the vertical betatron oscillations is increased by about $5^o/o$. With conventional magnets it is not too difficult to obtain such a homogeneity as long as the steel is not saturated. However, at 4.0 T the steel is completely saturated so that the field distribution is determined mainly by the geometry of the coils. It is instructive, therefore, to consider first some coil geometries without iron.

In the coil geometry shown in Fig. 8a the windings lie on a cylindrical surface and are assumed to be infinitely thin. Their distribution is such that the current between ϑ and $\vartheta + d\vartheta$ is

$$i \, d\vartheta = I/2 \cos\vartheta \, d\vartheta \qquad (12)$$

It can be shown that this gives a perfectly homogeneous field. In practice the windings have a considerable thickness and a more practical arrangement e.g. for coils that fit around the ISR vacuum chamber is shown in Fig. 8b. It can again be shown readily that with a uniform current density in the shaded area the field is perfectly homogeneous, but for the same width of the good field region and the same number of ampereturns the field in the coil of Fig. 8b is only $1/\pi$ times the field in the coil of Fig. 8a. Comparison of Fig. 8a and 8b suggests that there is a whole range of coil shapes in between these two, giving homogeneous fields. The optimum coil shape then depends on the current density that can be realised with the particular type of copper-clad or otherwise stabilized superconducting wire.

For superconducting magnets that should have a wide gap for the analysis of secondary particles the arrangement of Fig. 8c may be preferable. The field is mainly produced by the two large coils but there are also a number of smaller correcting coils with adjustable currents to obtain the required field homogeneity.

The forces on the conductors are very large. In a typical magnet as shown in Fig. 8c, with w = 1 m. and h = 0.5 m, at a field B = 4T, the attractive force between conductors with equal currents is about 250 tons/m and the repulsive force between conductors with opposite currents about 350 tons/m. These forces require strong supports and therefore the superconducting coils will certainly be considerably more voluminous than is suggested by the sketches of Figs. 8a to 8c. An important part of the design will in fact be, to make supports that obstruct as little as possible the trajectories of secondary particles that may also have to pass through the magnet. In an ironfree coil the coil bracings can also be inside the dewar and cooled down to liquid helium temperature.

The stray field at a distance of 5 m from an ironfree superconducting magnet with a field of 4 T and dimensions corresponding to magnets M_1 in the diagrams discussed below is of the order of 0.05 T. The extra flux density in a large mass of iron, like an ISR magnet unit would be a few times larger, since the iron tends to "suck in" the flux lines from the surrounding space. This would represent a major perturbation to the particle orbits in the ISR and has to be corrected.

One possibility would be to shield the stray field locally by surrounding the ISR magnet units and straight sections in the vicinity of the crossing point with large shells of steel or with large local correcting coils. Another approach would be, to surround the superconducting coils with additional coils that produce a weaker, oppositely directed field but which have larger dimensions. By an appropriate choice of parameters one can then obtain approximate cancellation of the stray fields at large distances. Such an arrangement tends to become rather voluminous and requires considerably more (say a factor 3) ampère turns for a given deflecting power of the superconducting magnet than the simple coil arrangement.

In general it appears desirable, and for special magnets that are close to the ISR magnet units it will certainly be necessary, to build a steel yoke around the large superconducting magnets in order to reduce the stray fields. This has the additional advantage of reducing the number of ampèreturns by about a factor 2. If the steel surface coincides with an equipotential surface of the magnetic field around the coils, where the maximum flux density is lower than the saturation value, no disturbance of useful field distribution should result at any field level. If the system is symmetrically built and the coil system is sufficiently rigid in itself, no forces will develop between the coils and the yoke. In fact the coils are in an unstable equilibrium position with respect to the yoke and moderately small supports should be sufficient to keep the coils in place. On the other hand it would be interesting to be able to take up the forces on the coils by strong supports from the yoke, thus eliminating obstructing spacers between the coils. However, strong supports with one extremity at room temperature and the other extremity at liquid helium temperature give rise to difficult engineering problems.

In view of the arguments given above, we have shown in the drawing discussed below the dotted outline of a steel return yoke of rectangular shape and with a cross-section that is just sufficient to carry the flux of the superconducting magnet with B = 2.0 T in the steel. More detailed studies of superconducting magnets could lead to a position or shape of the yoke that is somewhat different from those presented in our sketches.

4. Possible geometries for head-on collisions

In discussing some possible arrangements for head-on collisions we shall in general assume the use of superconducting magnets with a field of 4 T, but in some cases we shall also show the possible use of conventional magnets. There are two different approaches to the choice of the best layout. One would be, to make the special magnets as slender as possible and to place them as far as possible from the crossing point, so that they subtend a small solid angle and leave the maximum space free for experimentation. The alternative is to place the special magnets rather close to the crossing point and to give them the largest possible gap so that they are at the same time useful for momentum analysis of the secondaries. This is attractive since many secondaries will be produced at small angles.

Fig. 9 shows a layout for head-on collisions for structure 1 and Fig. 10 for structure 2. Both are based on the second alternative in III.2 In fact for structure 1 this seems to be the only possibility in the limited available straight section space. In both cases there are magnets M_3 and M_3' (not shown) in the a_4 straight sections, and the ISR magnet periods have been displaced laterally. The two sketches are very similar, but in Fig. 10 there is more free space between M_1 and the ISR magnet units, which may be very valuable for detectors. Magnets M_2 and M_3 can have a field of 1.5 T. As an exemple of what could be done if one is pressed for space, we have assumed that M_2 in Fig. 10 is placed against the F-unit of the ISR and has a common coil with it. Since M_2 has parallel poles, a gap height of 8 cm would be sufficient and therefore its field would be about 1.5 T for the same number of ampère-turns that give 1.2 T in the ISR unit. A similar arrangement would be possible, of course, in some of the other sketches.

Fig. 11 shows the equivalent of Figs. 9 and 10 for the 9° machine. In this case it is possible, to obtain head-on collisions with a conventional magnet with a field of 1.6 T, but one can also, of course, use a shorter superconducting magnet.

Fig. 12 shows an arrangement for head-on collisions in the 9° machine with all magnets in a_2. This would be a rather doubtful possibility for the 15° machines and even in the 9° machine the magnets take up most of the straight section spade.

In Fig. 13 the magnet M_1 has been placed as far as possible from the crossing point and it has been assumed that the beams cross at an angle of 1°. Even so M_1 with its return yoke subtends quite a large solid angle at the crossing point. M_2 which is close to the ISR magnet units will certainly need a return yoke and therefore the latter has been drawn in full lines.

Fig. 14 shows the corresponding arrangement for the 9° machine. Since the coils of the first magnet units of the ISR practically touch, we have allowed a crossing angle of 2.6° in order to place M_1 as far away from the crossing region as possible. In this case M_1 and M_2 can be picture frame magnets of conventional design and with a field of 2.0 T. They should take up considerably less lateral space than the corresponding magnets in Fig. 13.

5. Improvement of the interaction rate due to head-on collisions

If the two ISR beams cross at an angle ψ, the interaction rate is

$$I_1 = \left(\frac{N}{2\pi R}\right)^2 \cdot \frac{c\sigma}{h\ \mathrm{tg}\,\psi/2} \qquad (13)$$

where h = beam height and the other symbols are well known.

If the beams collide head-on or at a very small angle, in such a way, that they overlap over a distance L, the interaction rate is

$$I_2 = \left(\frac{N}{2\pi R}\right)^2 \cdot \frac{2\sigma c L}{hw} \qquad (14)$$

where w = beam width. The "geometrical" improvement factor F_1 due to head-on collisions is therefore

$$F_1 = R_2/R_1 = \frac{L\psi}{w} \qquad (15)$$

A single burst from the improved CPS will have a width of about 2 cm. If secondaries can usefully be collected from a length L = 1 m, the improvement due to the modified geometry is $F_1 = 13$ for $\psi = 15^{\circ}$ and $F = 8$ for $\psi = 9^{\circ}$.

The maximum intensity of a full stack is reduced by closed orbit distortions due to special magnets for head-on collisions and the Terwilliger scheme. If we define reduction factors f_c and f_t due to these effects, and assume that they are multiplicative, the overall improvement factor for the maximum interaction rate is

$$F_2 = f_c^2 \, f_t^2 \, \frac{L\psi}{w} \qquad (16)$$

It has not been possible in the limited time to make detailed calculations for all the geometries shown in Figs. 9 to 14. Orbit computations made for a number of representative cases show, that in general the betatron oscillations are affected in only a minor way, but that the closed orbits for off-momentum particles are somewhat deformed. In a typical case one finds $f_c = 0.8$ to 0.85 and therefore we shall take $f_c^2 = 0.70$.

For a full stack, which has a width of about 50 mm (for $\Delta p/p = 2^{\circ}/o$) + 20 mm (beam size) = 70 mm, we then find $F_2 = 2.6$ for $\psi = 15^{\circ}$ and $F_2 = 1.6$ for $\alpha \simeq 9^{\circ}$.

The Terwilliger scheme, that can be used to decrease w in the crossing region also reduces the maximum stacked intensity. If the Terwilliger quadrupoles are excited after stacking is finished (see eq. 10) we find $f_t = 0.76$ and therefore the interaction rate decreases by a factor $f_t^2 = 0.58$. However, now we have w = 2 cm, so that $F_2 = 5.3$ for $\psi = 15^{\circ}$ and $F_2 = 3.2$ for $\psi = 9^{\circ}$.

If one wants to use a small vacuum chamber in the crossing region, the Terwilliger quadrupoles must be excited before stacking starts. Even with the injector in the optimum azimuthal position the maximum stacked intensity is then reduced by a factor $f_t = 0.46$ and the interaction rate by a factor $f_t^2 = 0.21$. This leads to $F_2 = 2.0$ for $\psi = 15^0$ and $F_2 = 1.2$ for $\psi = 9^0$.

From these considerations we see, that with head-on collisions the interaction rate is increased by about one order of magnitude for single bursts from the CPS. This would be particularly significant if it were not possible to stack in the ISR. However, the same increase in interaction rate can be obtained if one stacks $\sqrt{F_1} \approx 3.5$ pulses in the ISR. Therefore the only gain achieved by head-on collisions is an improvement $\sqrt{F_1}$ in signal to noise ratio. One would, therefore, for particular experiments, want to consider other possible methods of achieving the same result before embarking on this rather elaborate method. It may, for instance, be more profitable to spend the effort on vacuum or on bunching. From the figures given above one also sees that for a full stack the increase in maximum interaction rate F_2 is only moderately larger than one. To this one has to dd the fact that with a larger volume of overlap of the two beams it may be somewhat more difficult to discriminate against background.

So far we have assumed that beam-beam effects are not limiting the obtainable interaction rate. Recent investigations indicate that this is a safe assumption for the ISR performance as estimated in reference [1)] and with normal 15^0 or 9^0 crossings. However, if one increases substantially the length of overlap at one crossing point, the beam-beam interaction will certainly become stronger, increasing the probability of getting instabilities. This may constitute a fundamental limit to the obtainable interaction rate, and may reduce the usefulness of head-on collisions.

6. Layouts for intermediate crossing angles

The large magnets shown in Figs. 9 to 14 represent serious obstructions to the secondary particles that one wants to study and, as shown above, lead to only moderate advantages. Although such an attempt must be rather speculative we have therefore tried to see if modifications of the special magnets discussed above might offer advantages.

It seems likely that there will always be a need for large acceptance magnets to analyze secondary particles. Since the analyzing fields must be close to the ISR vacuum chamber anyhow, the design of these magnets is simplified by allowing that they also act on the circulating beam. Therefore it seems reasonable to admit substantial variations in the crossing angle.

One possible arrangement for the 9° structure, which follows these ideas is shown in Fig. 15. Magnet M_1 deflects the ISR beams over 40 mrad and therefore reduces the crossing angle from 9° to 4.5°. In the direction perpendicular to the ISR beams, its gap width is 3 m, while the distance from yoke to yoke is 4.5 m. The permissible gap height is limited by the fact that a very large gap will lead to a rather inhomogeneous field that upsets the betatron oscillations in the ISR. More detailed studies are necessary to settle this point, but gap heights of the order of 1 m may be possible.

The corresponding drawings for structures 1 and 2 are shown in Figs. 16 and 17 respectively. In all these three drawings we assume that magnet M_1 has the same characteristica and is at the same distance from the crossing point. To illustrate the flexibility offered by a large crossing angle, we assume that at the same time the first F and D magnet unit downstream of the crossing point has been replaced by a special section as shown in Fig. 6. Magnet M which has an extended gap would again be used to analyse protons that are scattered over small angles and have lost too little energy to be separated from the circulating beam by M_1. The small magnet M_2 should in Figs. 16 and 17 have a deflection of about 15 mrad. We have therefore assumed that

M is made slightly larger compared to Fig. 6, i.e. that it has a length of 4.5 m instead of 4.0 m, and that its field is increased from 1.45 T to 1.6 T. This should be permissible if we assume, that M is centered on the beam, which is reasonable in this case, since one is equally interested in particles that are scattered to the right and to the left. In the 9° structure there is no space for a large magnet M, unless the field of M_1 is reversed and the crossing angle is increased from 9° to 13.5°.

IV. Comparison of the ISR Structures

In the following chapter the advantages and disadvantages of the ISR structures no. 1, 2, and 4 are listed and commented upon. We have tried to express the important differences between them in the form of figures which are given in Table 5. Some explanation of the table entries are given in the footnotes below.

Table 5. Comparison of ISR Structures

Structure no.	1	2	4
Maximum energy	28	26.6	28 GeV
Intersection angle	15°	15°	9°
Length of intersection region	16.78	18.71	20.0 m
Number of magnet types[1)]	4	4	2
Number of coil types[1)]	4	4	2
Auxiliary windings on long units[2)]	yes	yes	no
Total no. of straight sections[3)]	132	132	80
Total no. of pickup stations[3)]	48	48	44
No. of pickup stations inside radial field magnets[3)]	0	0	8
Required vertical aperture	49	53	57 mm
Additional cost[4)]	0	~ 2	6-7 Msfr
Space available for septum magnet[5)]	9.40	9.50	9.55 m
Zero angle possible without displaced periods and:	advanced sup.cond.		sup.cond.
Zero angle possible with displaced periods and:	sup.cond.		steel magn.
Beam height in intersection regions	9.6	10.1	13.1 mm
Gain in interaction rate (under normal crossing angle condition)	0	-5	+23 %
Minimum distance between orbits at the position of the first inner magnets[6)]	2.50	2.50	1.54 m
Layout of intersection regions without special magnets	Fig. 18		Fig. 1
Layout of intersection regions with special magnets	Fig. 6		Fig. 6

1) In the 15° structure the number of magnet types is twice that of the 9° structure because there are long and short units, also the coils will be of four types: two long and two short. This is a drawback from the point of view of magnet engineering, but the necessary technical solutions have been presented in the design study report[1].

2) Since the fringe field effects will vary differently with field level whether the magnet end faces an open space or another magnet nearby, auxiliary windings must be foreseen on the long units in order to make the bending angles of all magnets equal at all field levels. This is a small complication from an operational point of view.

3) Since the number of straight sections is much smaller in the 9° structure than in the 15° ones, the number of beam observation electrodes had to be reduced to 44, 8 of which are inside radial field magnets. Despite this effort of saving straight sections, there is no mid-D space available for spare quadrupoles to tune the machine in the 9° structure. If such correcting quadrupoles turn out to be necessary other equipment will have to be removed, which may not be easy. This is an example of the general relative disadvantage of the 9° structure that it has altogether less total field free space available for auxiliary devices.

4) The following facts contribute to the increase in cost between structures no. 1 and 4:

Increase in weight and cost of magnet steel	+ 1.4 MSfr.
Increased cost of blockmaking	+ 0.7 "
Increased weight and cost of coils	+ 1.6 "
Increase in power dissipation and cooling capacity	+ 1.6 "
Increase in size of correcting lenses	+ 0.8 "
Savings on girders and auxiliary windings	- 1.1 "
	5.0 MSfr.

These figures are based on the assumptions that

i) the gap height is increased by 10°/o

ii) the tunnel width and height remain the same

iii) the unit prices remain constant

From a machine point of view the tunnel width and height could be reduced. This would reduce the increase in cost by the following amounts:

Reduction in tunnel width by 1	0.9 MSfr.
Reduction in beam height by 0.2 m	0.2 "
Cranes	0.3 "
	1.4 MSfr.

These modifications would limit the additional cost to 3.6 MSfr. However, they may not be desirable for experiments in the intersection regions with normal tunnel cross sections.
In addition to the cost increase on the machine components, there will be a cost increase estimated at 2 MSfr. due to the extra study required to bring structures 4, and possibly 2, to the same degree of advancement in the design as structure 1 is now. Since this requires extra time, leading to a delay of the project of about 6 months, the yearly budgets may not be higher than the presently estimated ones.

5) From an injection point of view all three structures are very similar. However, the phase advance between the septum and the kicker is slightly more convenient in no. 4 resulting in a small reduction of their strengths. For beam dumping and ejection structure no. 4 has advantages over the other two.

6) For the sake of brevity the information about the space available between inner and outer arc is cast into a single figure. The detailed information on the geometry of the intersection regions is shown in the figures referenced in Table 5.

In conclusion, from a technical point of view there is little difference between the three structures. Structure 4 has a somewhat simpler magnet system and more convenient ejection, nos. 1 and 2 have slightly more convenient arrangement of beam-observation stations, to mention some differences. However structure 4 is clearly more expensive.

From a physics point of view the main differences are that structure 4 requires less total bending power to reach zero degree and has about $20^{o}/o$ longer straight sections in the interaction regions. This is counterbalanced by the fact that the structure leaves very little room for experimental devices, special magnets included, between the magnet units near the ends where the inner and outer arcs approach each other. In this respect structures 1 and 2 leave much more flexibility. This fact is illustrated clearly in Figs. 1 and 18. We attached much significance to this argument when we first chose a structure with 15^{o} crossing angle for our detailed study presented in[1)]. Since this preference for structure 1 crystallized itself long ago, the design based on this structure is, of course, quite advanced, and a change away from it would now imply a delay. This should carry little weight in the choice, but the flexibility in detecting particles at small angles is still considered to be a very important argument in favour of structure 1, and is the main reason why we continue to recommend it rather than structure 4.

We also favour 1 rather than 2 on the ground that it is a pity not to make full use of the energy potentiality of the CPS in order to gain 2 m straight section length in the interaction regions.

APPENDIX

The simplest structure of ISR with different crossing angles which corresponds to practical requirements has outer arcs composed of three parts: a compact lattice, which produces the maximum possible orbit curvature, in the middle, and two straight sections at the ends. The inner arcs will, of course, also have straight sections near the crossing points, but since they have also other straight sections of about the same length elsewhere, their geometry is adequately represented, in first approximation, by an average radius of curvature, which is much larger than that of the compact lattice.

Figure 19 illustrates the geometry of this structure: α_1 and α_2 are the bending angles in the arcs of radius R_1 (outer) and R_2 (inner) respectively; ψ_y and ψ_x are the crossing angles, y is the outer straight section length at the point of crossing angle ψ_y (we call ψ_y the larger of the two angles), x is the outer straight section length at the point of crossing angle ψ_x.

The required superperiodicity of 4 imposes the condition $\alpha_1 + \alpha_2 = 90^\circ$. Assuming all magnet periods to have the same bending power, and calling N_1 the number of periods in the outer arcs and N_2 the number of periods in the inner arcs, we have:

$$\alpha_1 = \frac{N_1}{N_1 + N_2} \cdot 90^\circ \qquad \alpha_2 = \frac{N_2}{N_1 + N_2} \cdot 90^\circ$$

It can easily be seen that

$$\psi_y + \psi_x = \alpha_1 - \alpha_2 = \frac{N_1 - N_2}{N_1 + N_2} \cdot 90^\circ$$

If the two rings are identical, the system of the two is symmetrical with respect to the interaction points. The system has then 8 axes of symmetry, passing through the 8 crossing points. They cross at 45° from each other at a point 0, which can be called the "centre" of the ISR, but the crossing points ψ_y are not at the same distance from the centre as the crossing points ψ_x (the distance is smaller for the points with smaller crossing angle).

In general, R_1 is determined by the field and space requirements in the compact lattice, and the straight sections y and x must be long enough to avoid interference between the equipment of the two rings, the magnets in particular. The following geometrical relations can be written:

$$\begin{cases} (R_1 \tan \frac{\alpha_1}{2} + y) \sin (\frac{\alpha_2}{2} + \psi_y) = (R_1 \tan \frac{\alpha_1}{2} + x) \sin (\frac{\alpha_2}{2} + \psi_x) \\ 2R_2 \sin \frac{\alpha_2}{2} = (R_1 \tan \frac{\alpha_1}{2} + y) \cos (\frac{\alpha_2}{2} + \psi_y) + (R_1 \tan \frac{\alpha_1}{2} + x) \cos (\frac{\alpha_2}{2} + \psi_x) \end{cases}$$

from which x and R_2 can be determined, once R_1 and y have been chosen.

A certain number of practical cases have been computed, in particular:

$N_1 = 7 \quad N_2 = 5$, which corresponds to $\frac{\psi_y + \psi_x}{2} = 7^\circ 30'$

with the choice $\psi_y = 10^\circ 45' \quad \psi_x = 4^\circ 15'$

$N_1 = 7 \quad N_2 = 4$, which corresponds to $\frac{\psi_y + \psi_x}{2} = 12\ 3/11^\circ$

with the choice $\psi_y = 16^\circ \quad \psi_x = 8\ 6/11^\circ$

The results are shown in Table 6. Figures 20 and 21 show in detail the structures for the cases $\psi_y = 10^\circ 45'$, $\psi_x = 4^\circ 15'$ and $\psi_y = 16^\circ$, $\psi_x = 8\ 6/11^\circ$ respectively.

In all cases the straight section y, corresponding to the larger crossing angle ψ_y, has been given a value between 5.5 and 6 m, which gives a minimum free space of 4.5 to 5 m between the crossing point and the coils of the first lens. The straight section x has always come out larger than 20 m.

This has two important consequences:

1) The total straight section length at the small-angle crossing is in every case of the order of 30 m, taking into account the necessary free space in the inner arc as well. Therefore β has a large modulation and the vertical aperture has to be increased considerably with respect to the corresponding symmetric structure.

2) The space available for magnets and normal straight sections is smaller than in the symmetric structures. In the first of the two examples, which has the smallest crossing angle, the straight sections in the inner arc turn out so short that injection and ejection are very difficult and space for some correcting lenses is missing. In the other case, the total length of the magnets, and consequently the maximum momentum, is reduced.

TABLE 6

Geometrical Parameters of Asymmetric ISR Structures

Periods in outer arc	N_1	7	7
Periods in inner arc	N_2	5	4
Average of crossing angles	$\frac{\psi_y + \psi_x}{2}$	$7^\circ 30'$	$12\frac{3}{11}^\circ$
Large crossing angle	ψ_y	$10^\circ 45'$	16°
Small crossing angle	ψ_x	$4^\circ 15'$	$8\frac{6}{11}^\circ$
Radius of outer arc	R_1	101.6 m	93.94 m
Radius of inner arc	R_2	177.2 m	201.49 m
End s.s. of outer arc at ψ_y	y	6.0 m	5.62 m
End s.s. of outer arc at ψ_x	x	20.6 m	21.02 m
Maximum momentum	P_{max}	28 GeV/c	25.8 GeV/c
Maximum horizontal β		50.3 m	38.7 m
Maximum vertical β		98.2 m	82.8 m
Vertical β in interaction regions		30.6 m	26.7 m
Vertical aperture		88 mm	72 mm
Horizontal aperture		158 mm	140 mm

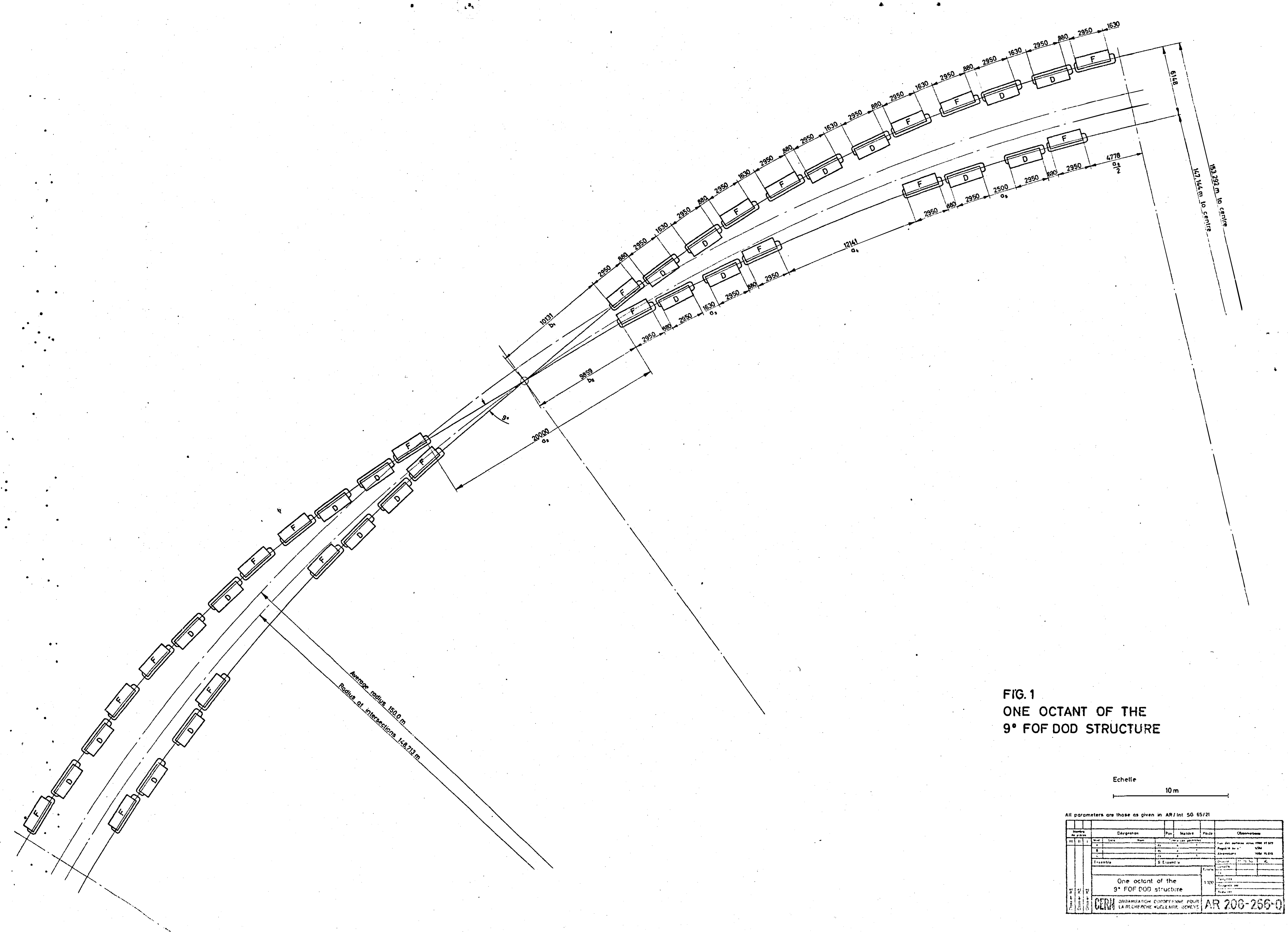

FIG. 1
ONE OCTANT OF THE
9° FOF DOD STRUCTURE

SIS/R/12040

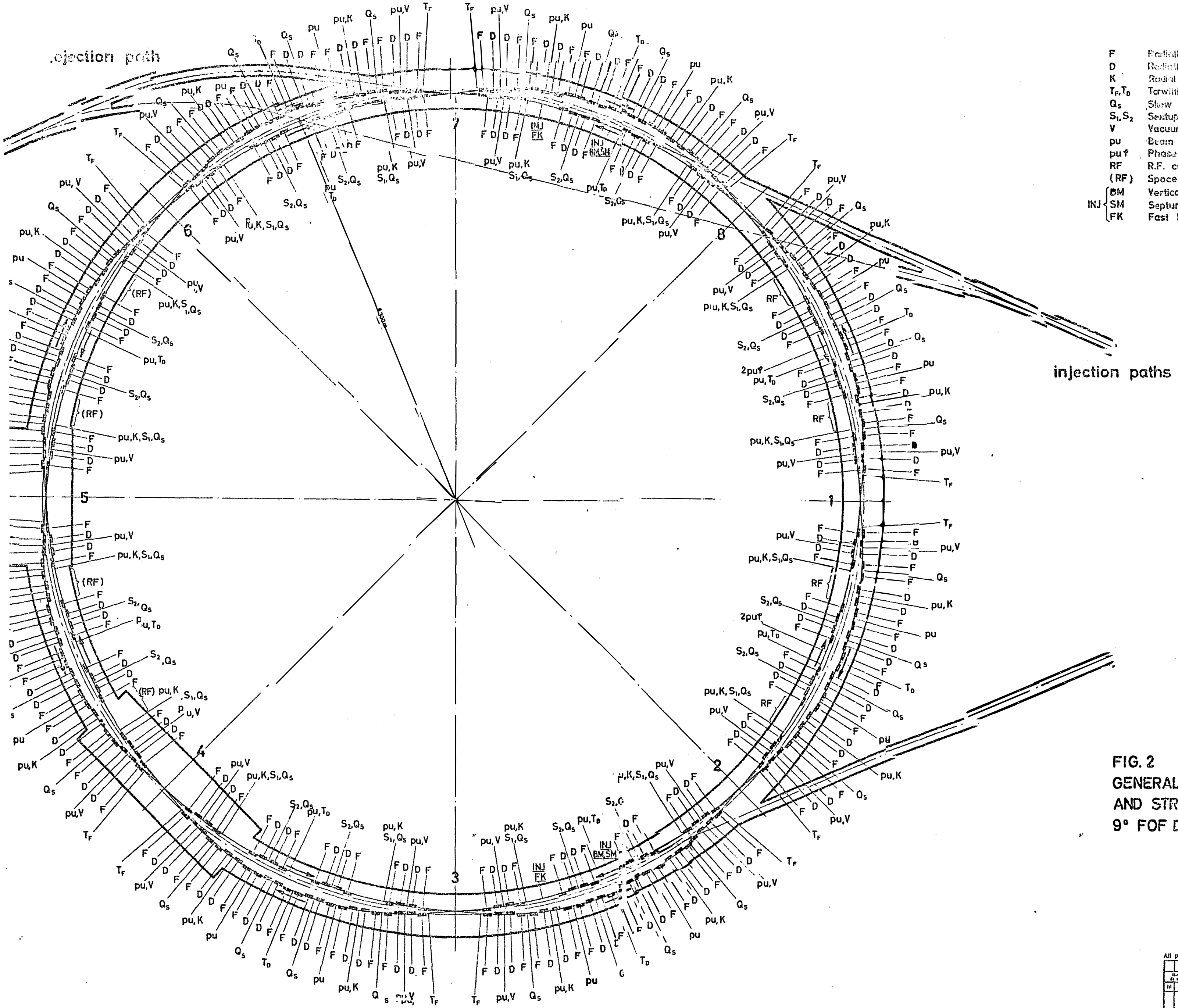

FIG. 2
GENERAL LAYOUT OF MAGNETS AND STRAIGHT SECTIONS IN THE 9° FOF DOD STRUCTURE

Echelle

50 m

All parameters are those as given in AR/Int. SG 65/21

General layout of magnets and straight sections in the 9° FOF DOD structure

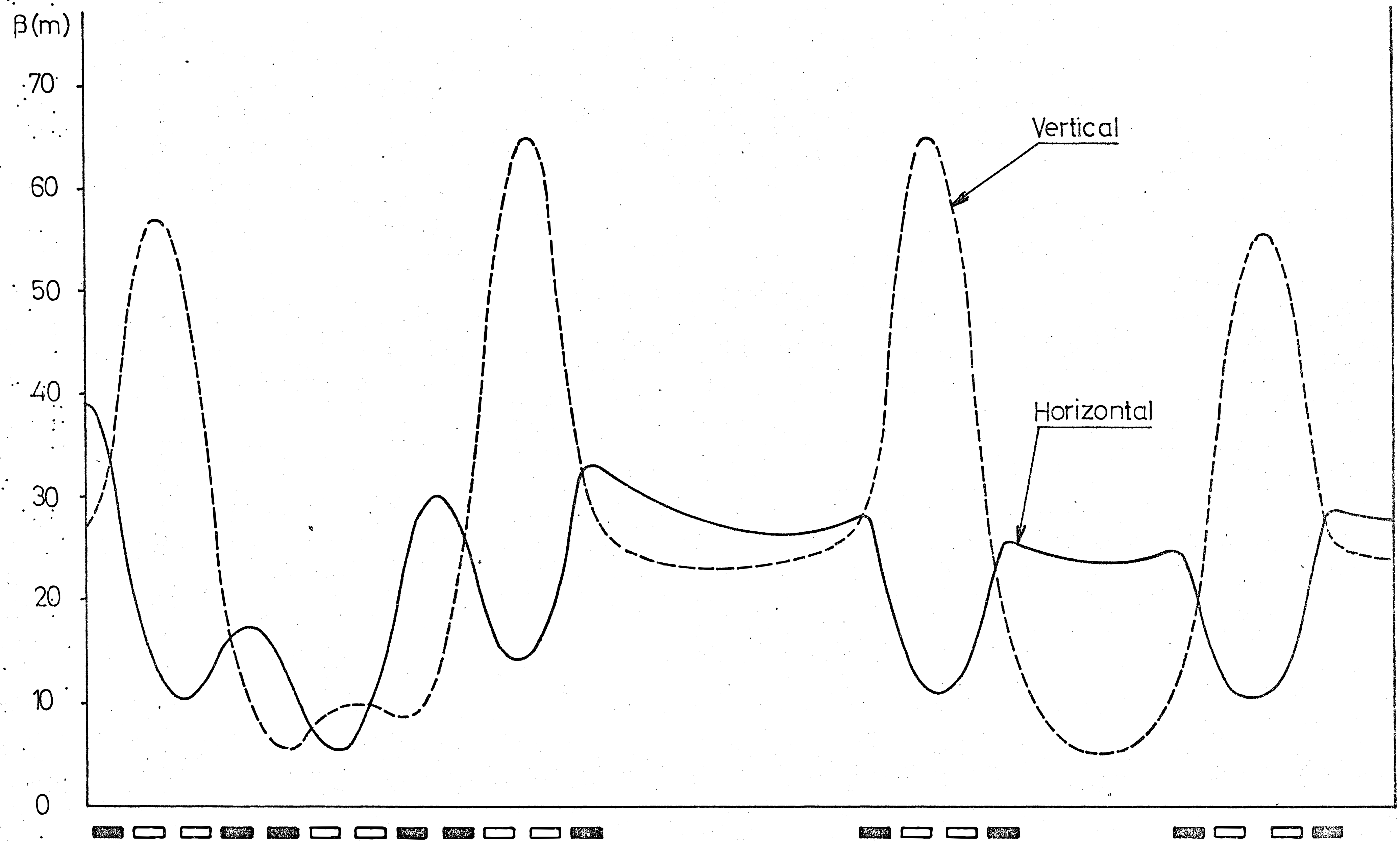

Fig. 3 VARIATION OF β OVER HALF A SUPERPERIOD IN THE 9° FOFDOD STRUCTURE

SIS/R/12046

SIS/R/12045

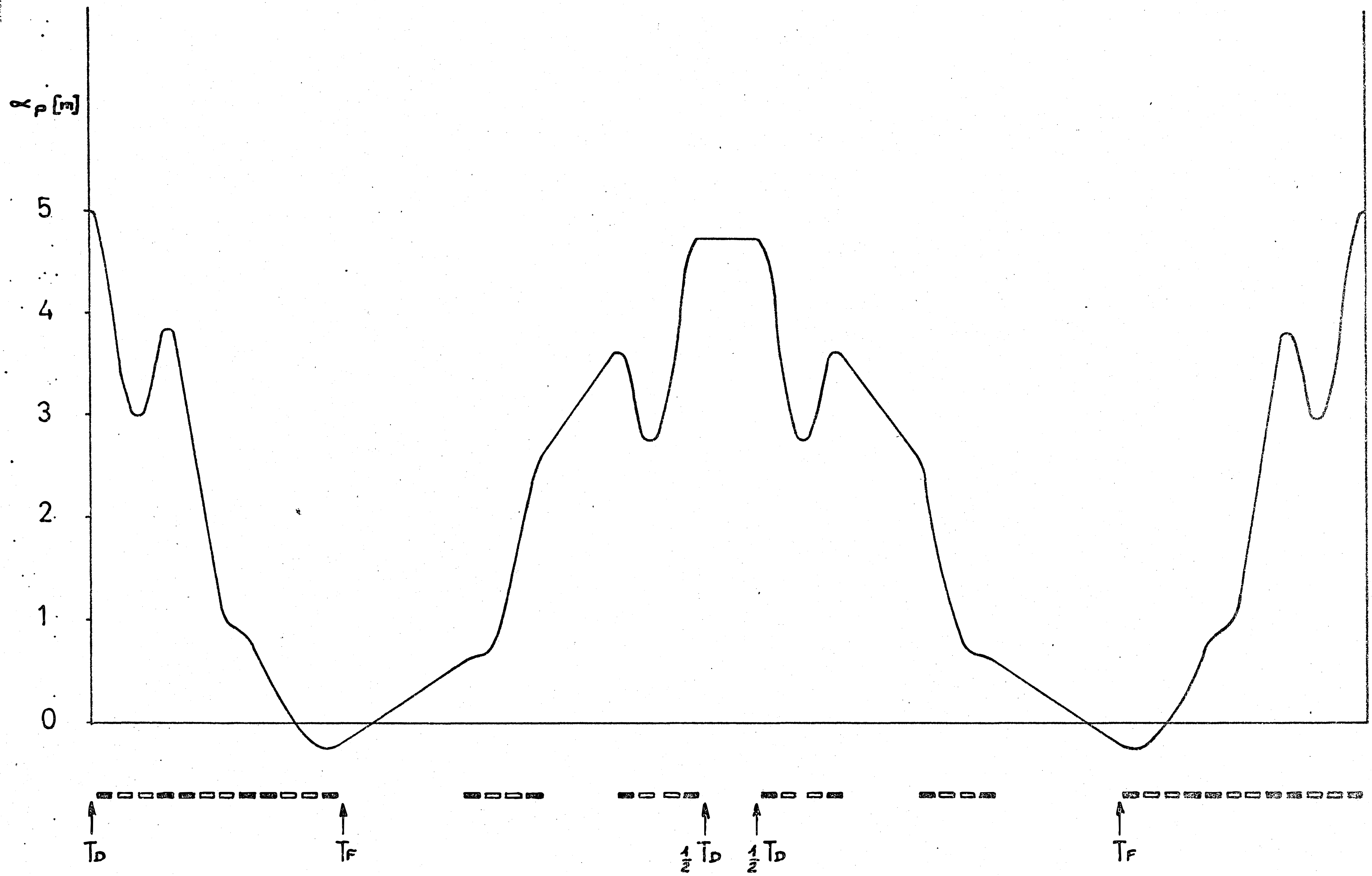

Fig. 4 MOMENTUM COMPACTION WITH TERWILLIGER SCHEME IN 9° FOFDOD STRUCTURE

SIS/R/12047

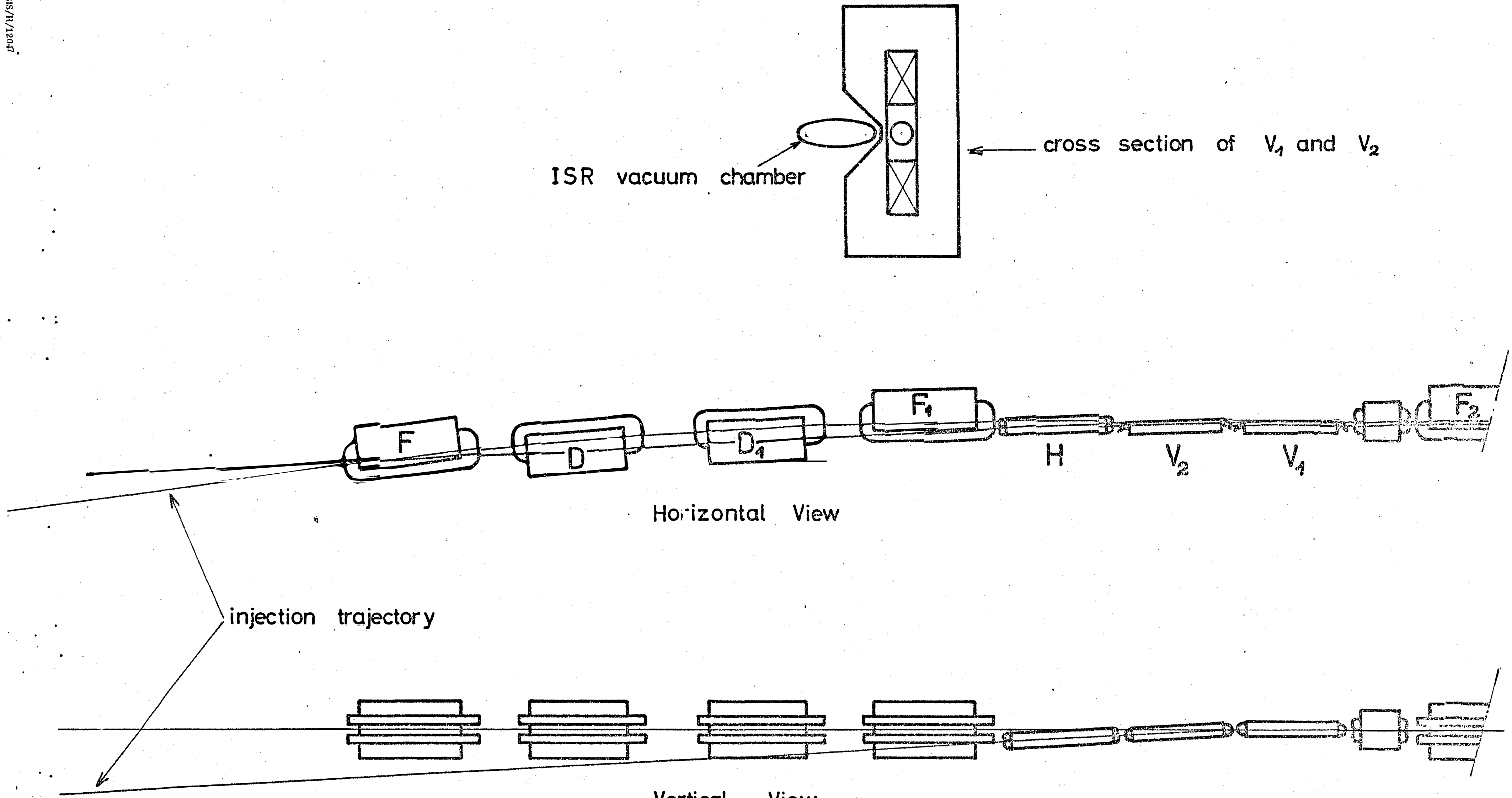

Fig. 5 Layout of the injection trajectory

SIS/R/12042

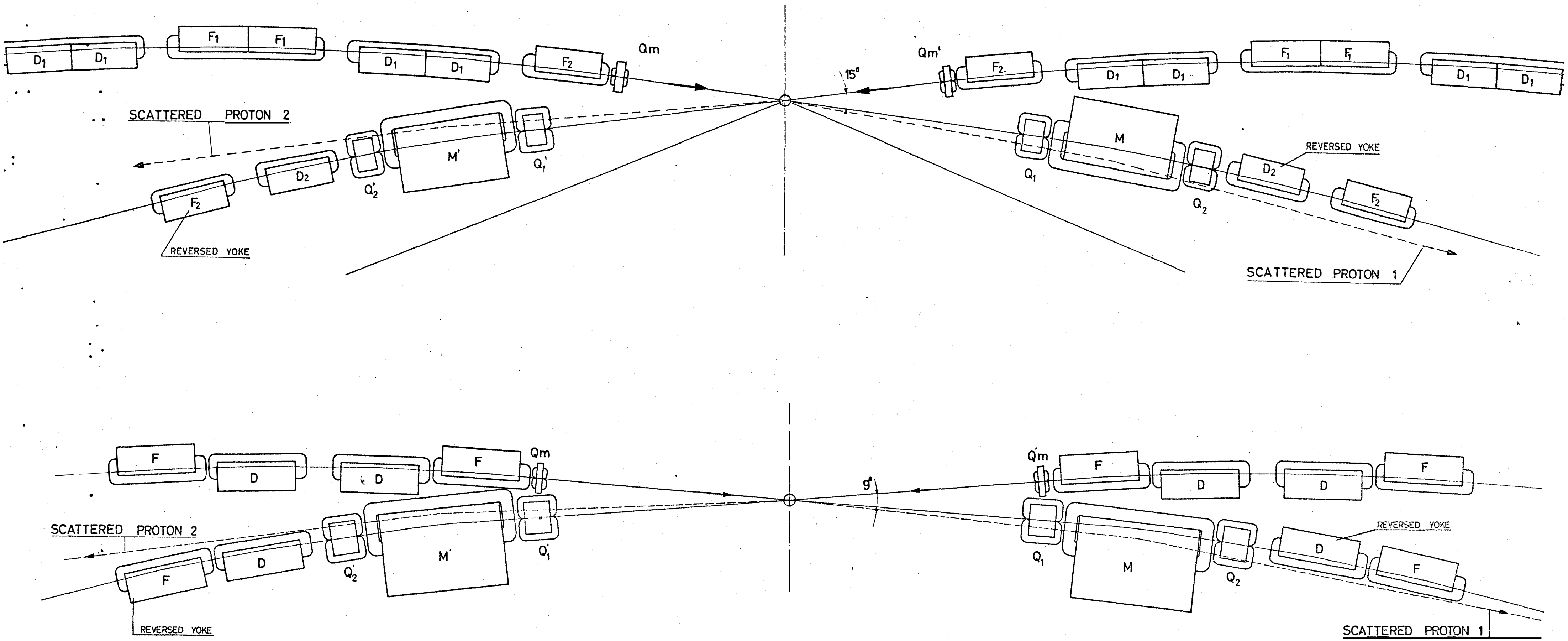

FIG. 6 SPECIAL MAGNET SECTIONS FOR SMALL ANGLE SCATTERING IN THE 15° AND 9° MACHINES

ALL PARAMETERS ARE THOSE AS GIVEN IN AR/INT SG/65-21

SPECIAL MAGNET SECTIONS FOR SMALL ANGLE SCATTERING IN THE 15° AND 9° MACHINES

CERN ORGANISATION EUROPÉENNE POUR LA RECHERCHE NUCLÉAIRE GENÈVE

AR 208-254-0

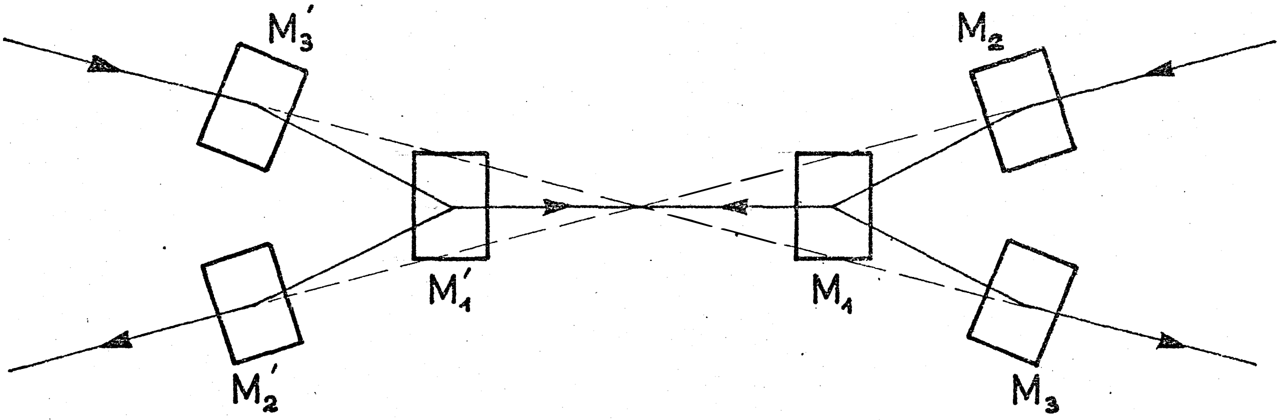

Fig. 7a Head - on collisions with all magnets in the crossing straight section

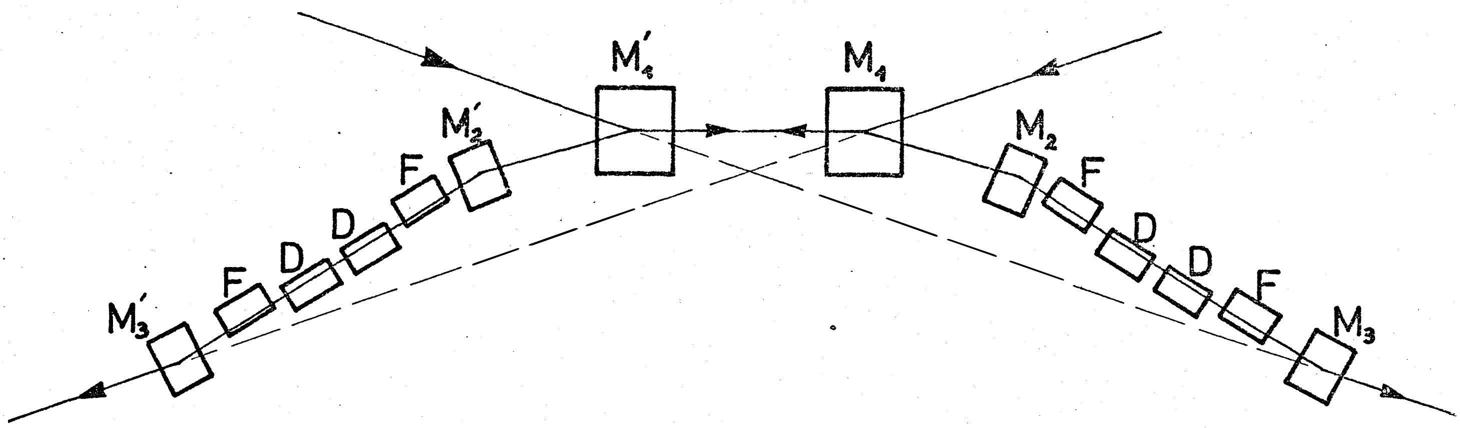

Fig. 7b Head - on collisions with laterally displaced ISR magnet units

SIS/R/12...

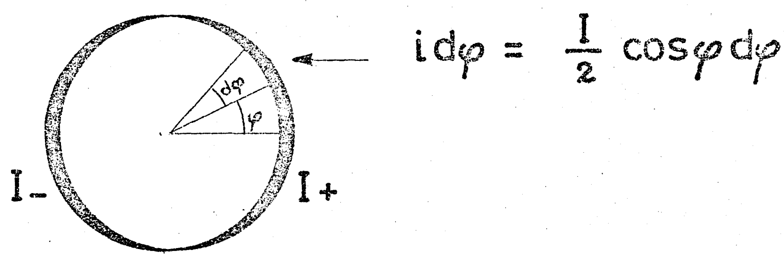

Fig. 8a   Cosine - like current distribution for homogeneous field

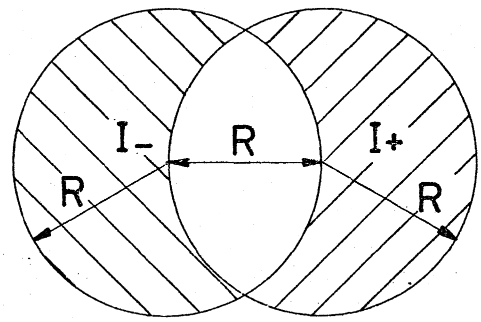

Fig. 8b   Homogeneous field production with two half - moon shaped coils

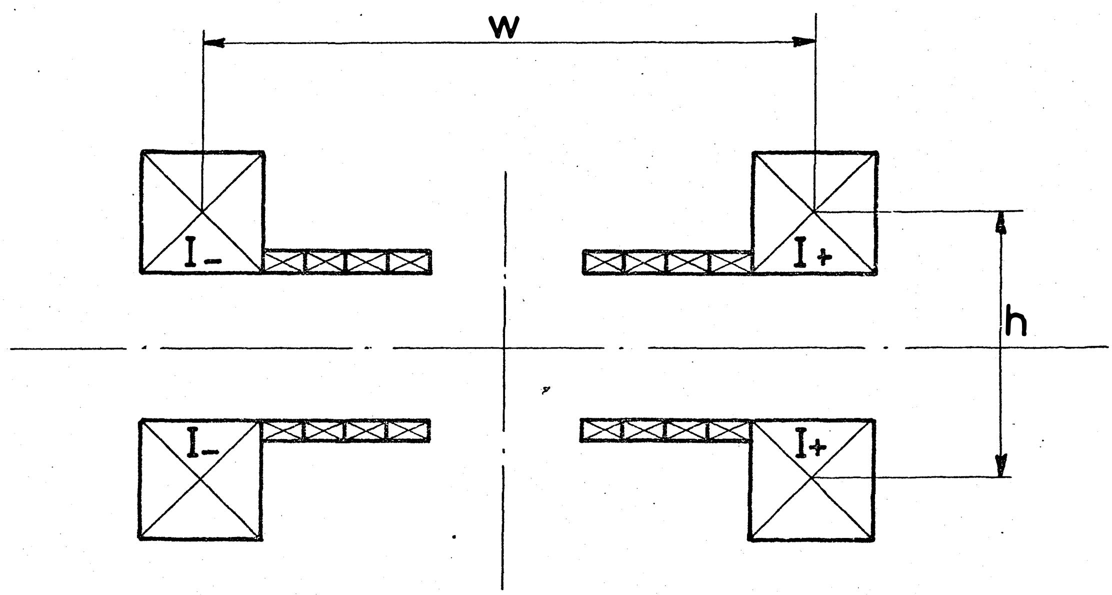

Fig. 8c   Homogeneous field production with main coils and correcting coils

SIS/R/12043

SIS/R/12039

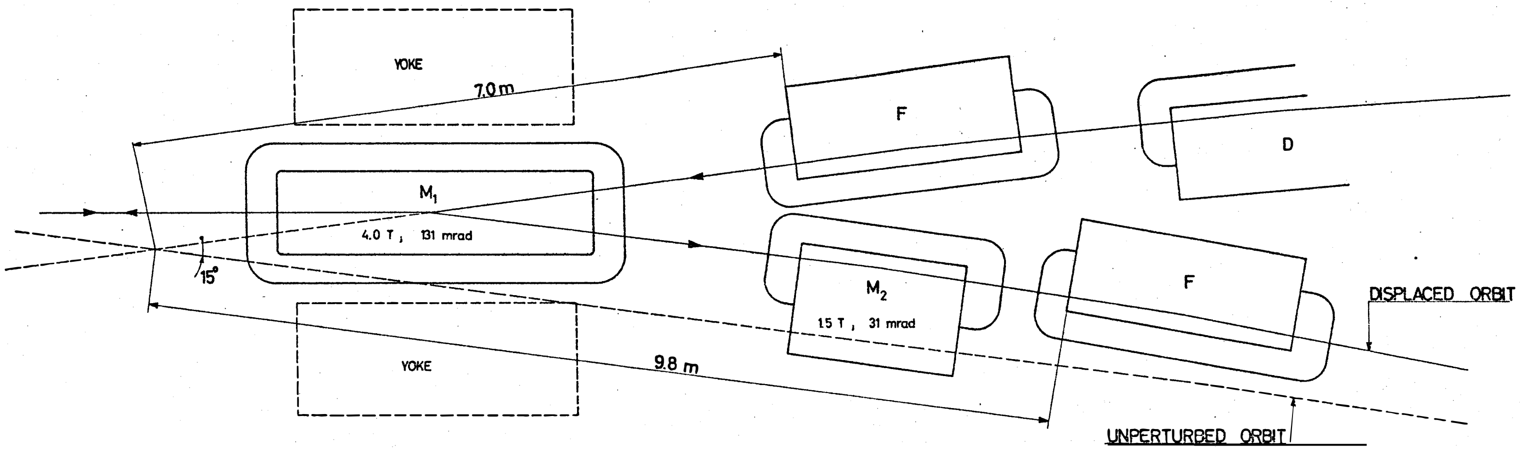

FIG. 9 HEAD-ON COLLISIONS IN 15° MACHINE, VERSION 1, WITH DISPLACED MAGNET UNITS

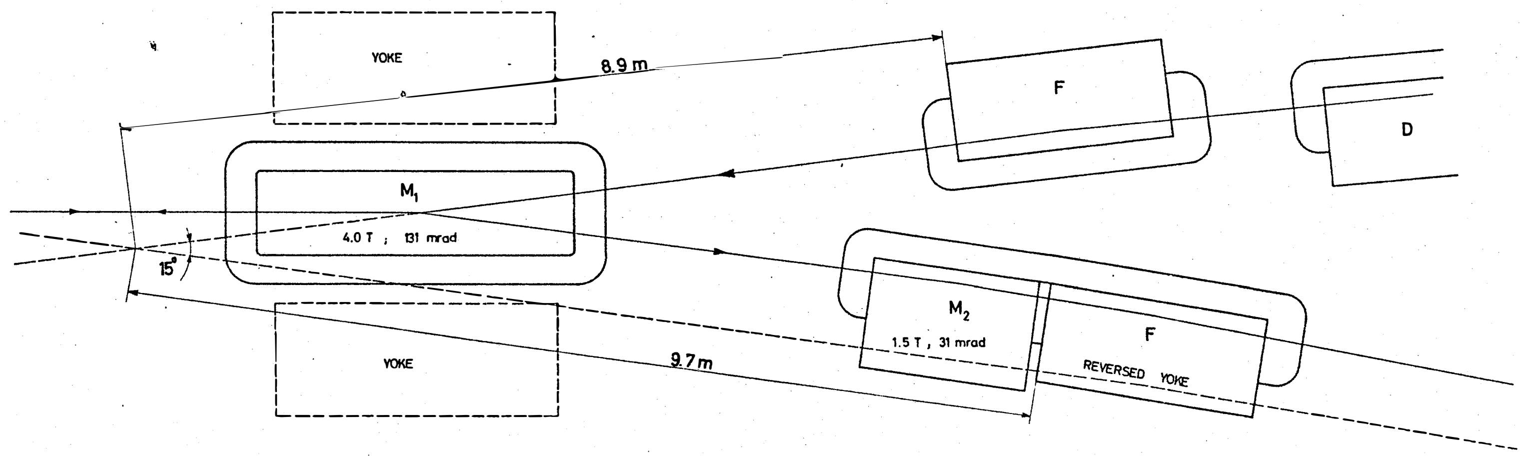

FIG. 10 HEAD-ON COLLISIONS IN 15° MACHINE, VERSION 2, WITH DISPLACED MAGNET UNITS

ALL PARAMETERS ARE THOSE AS GIVEN IN AR/Int SG/65-21

HEAD ON COLLISIONS IN 15° MACHINE VERSION 1, 2 WITH DISPLACED MAGNET UNITS

SIS/R/12035

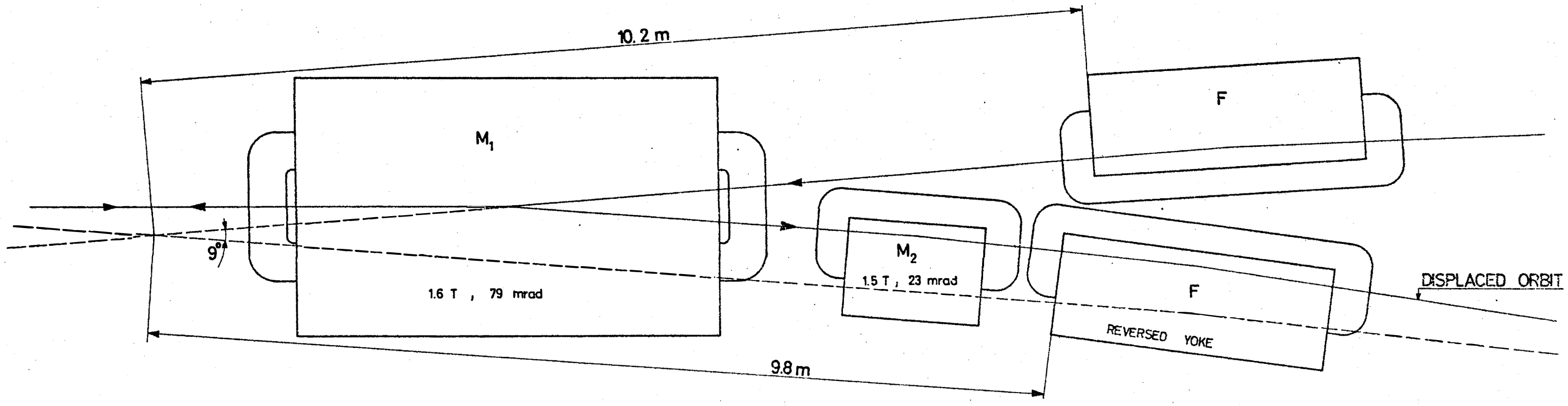

FIG. 11 HEAD-ON COLLISIONS IN 9° MACHINE WITH M$_1$ AS CONVENTIONAL STEEL MAGNET

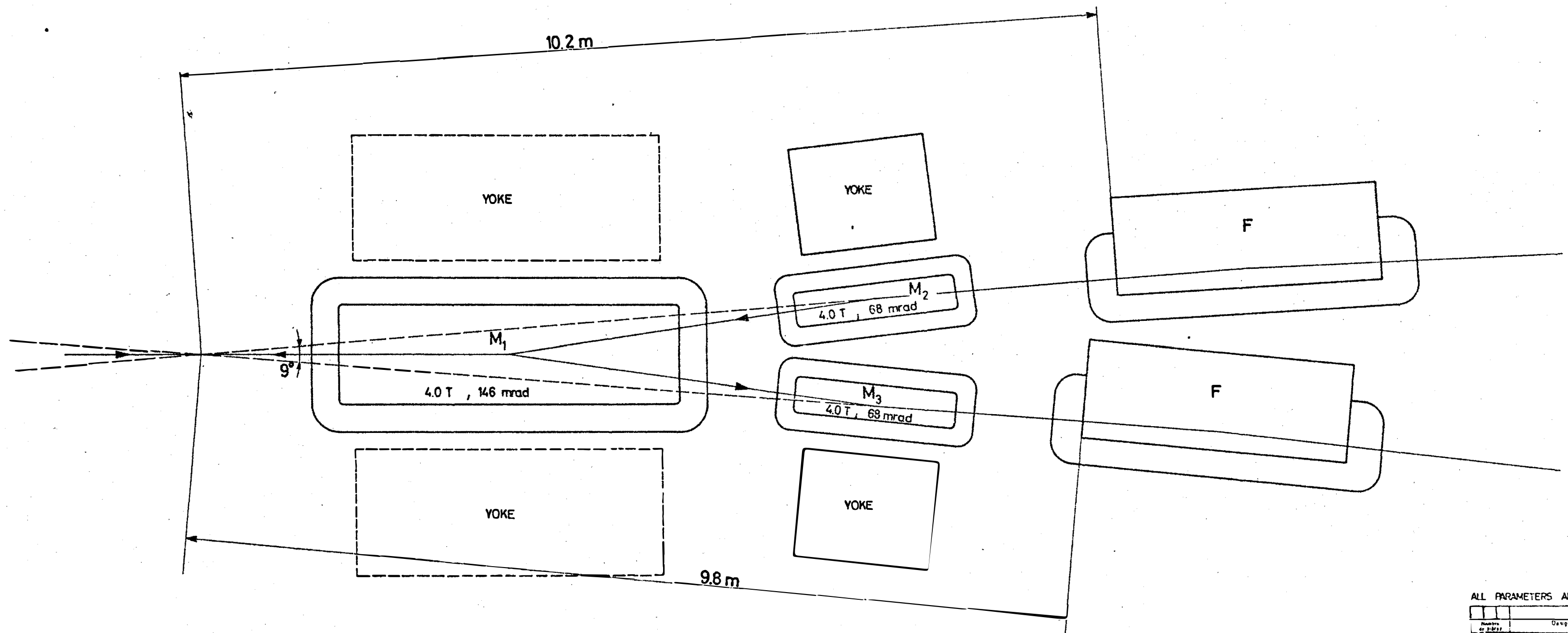

FIG. 12 HEAD-ON COLLISIONS IN 9° MACHINE, ALL MAGNETS IN CROSSING STRAIGHT SECTION

ALL PARAMETERS ARE THOSE AS GIVEN IN AR/NT SG/65.21

HEAD-ON COLLISIONS IN 9° MACHINE

CERN ORGANISATION EUROPÉENNE POUR LA RECHERCHE NUCLÉAIRE, GENÈVE AR 200-268-0

SIS/R/12087

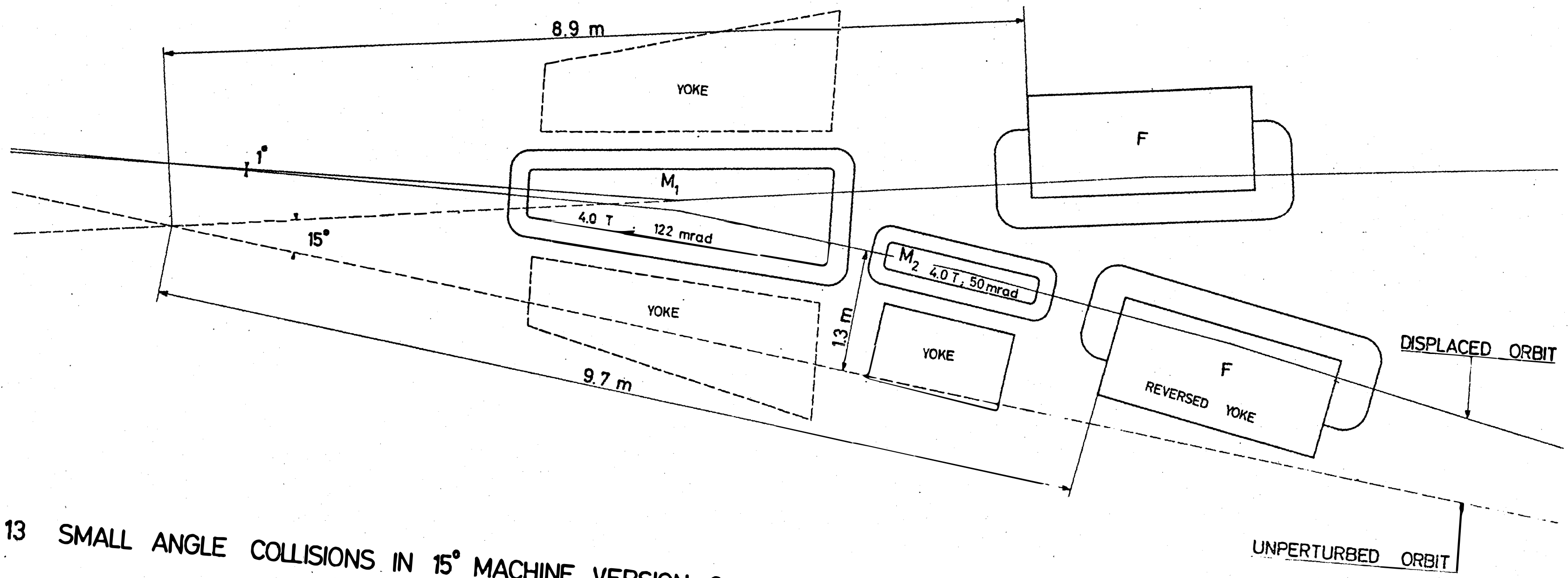

FIG. 13 SMALL ANGLE COLLISIONS IN 15° MACHINE, VERSION 2, M_1 AWAY FROM CROSSING POINT

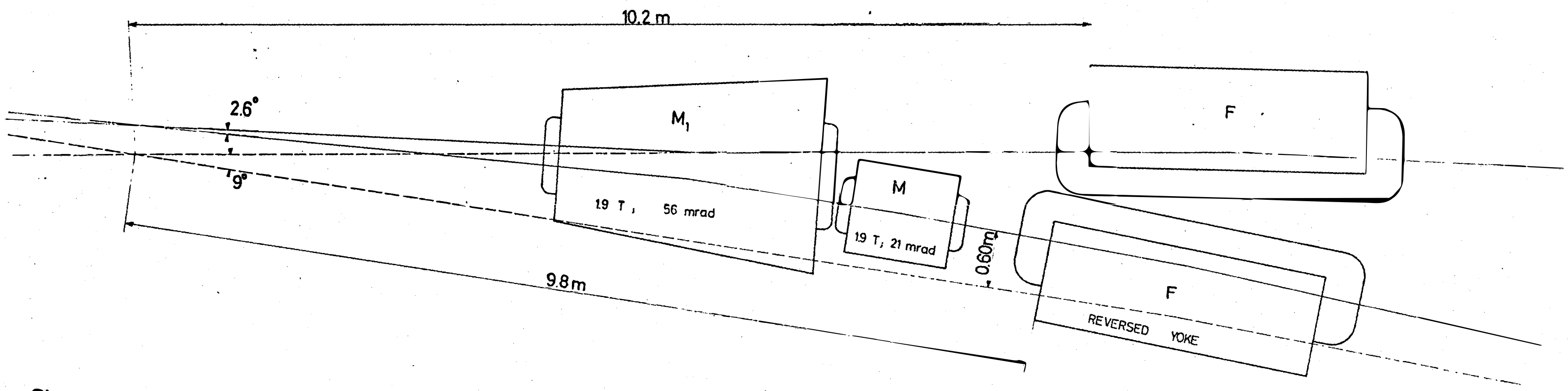

FIG. 14 SMALL ANGLE COLLISIONS IN 9° MACHINE, M_1 AWAY FROM CROSSING POINT

SIS/R/12036

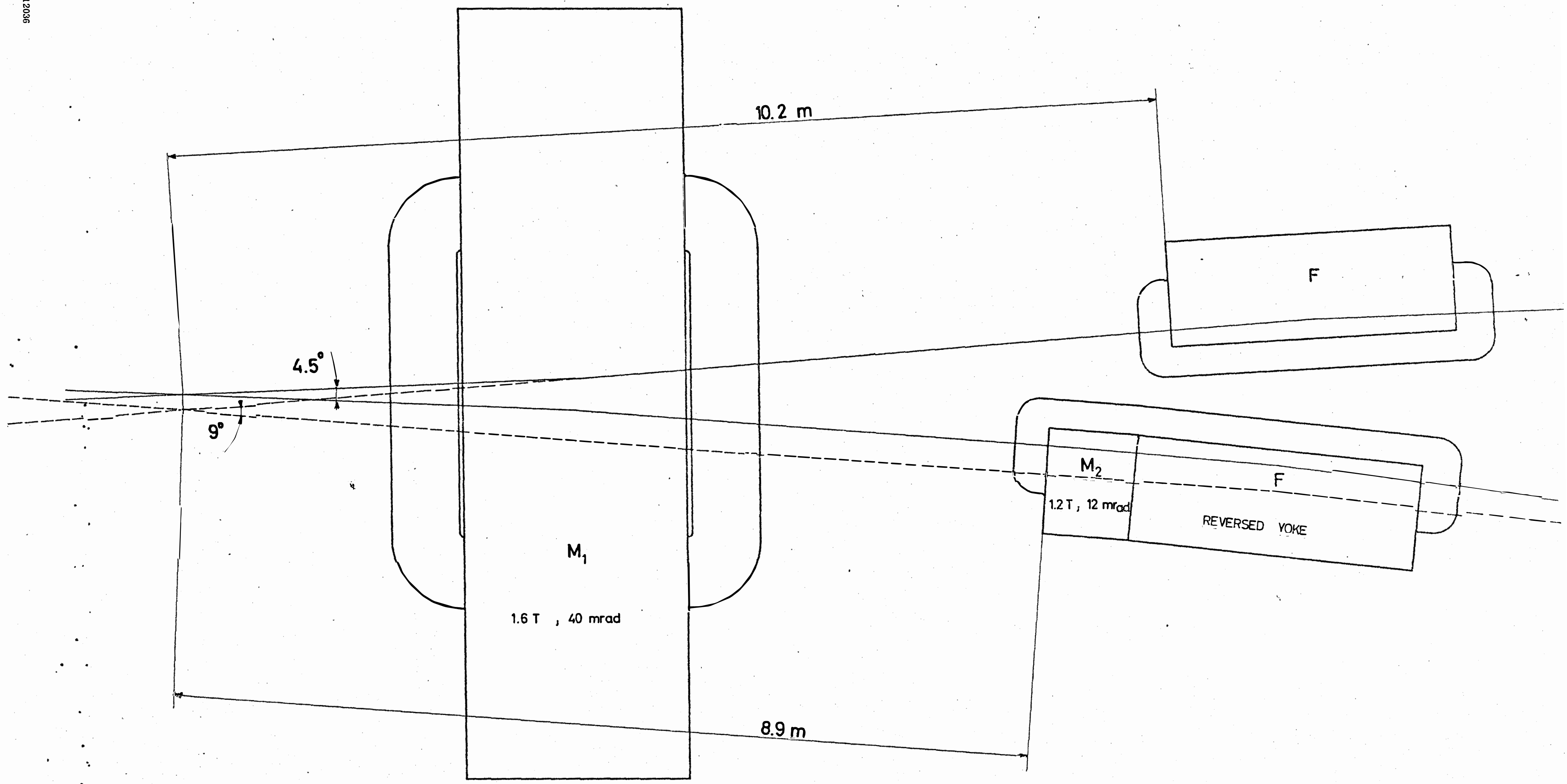

ALL PARAMETERS ARE THOSE AS GIVEN IN AR/INT SG/65-21

FIG. 15 STRUCTURE 4 WITH REDUCED CROSSING ANGLE

STRUCTURE 4 WITH REDUCED CROSSING ANGLE

CERN ORGANISATION EUROPÉENNE POUR

SIS/R/12038

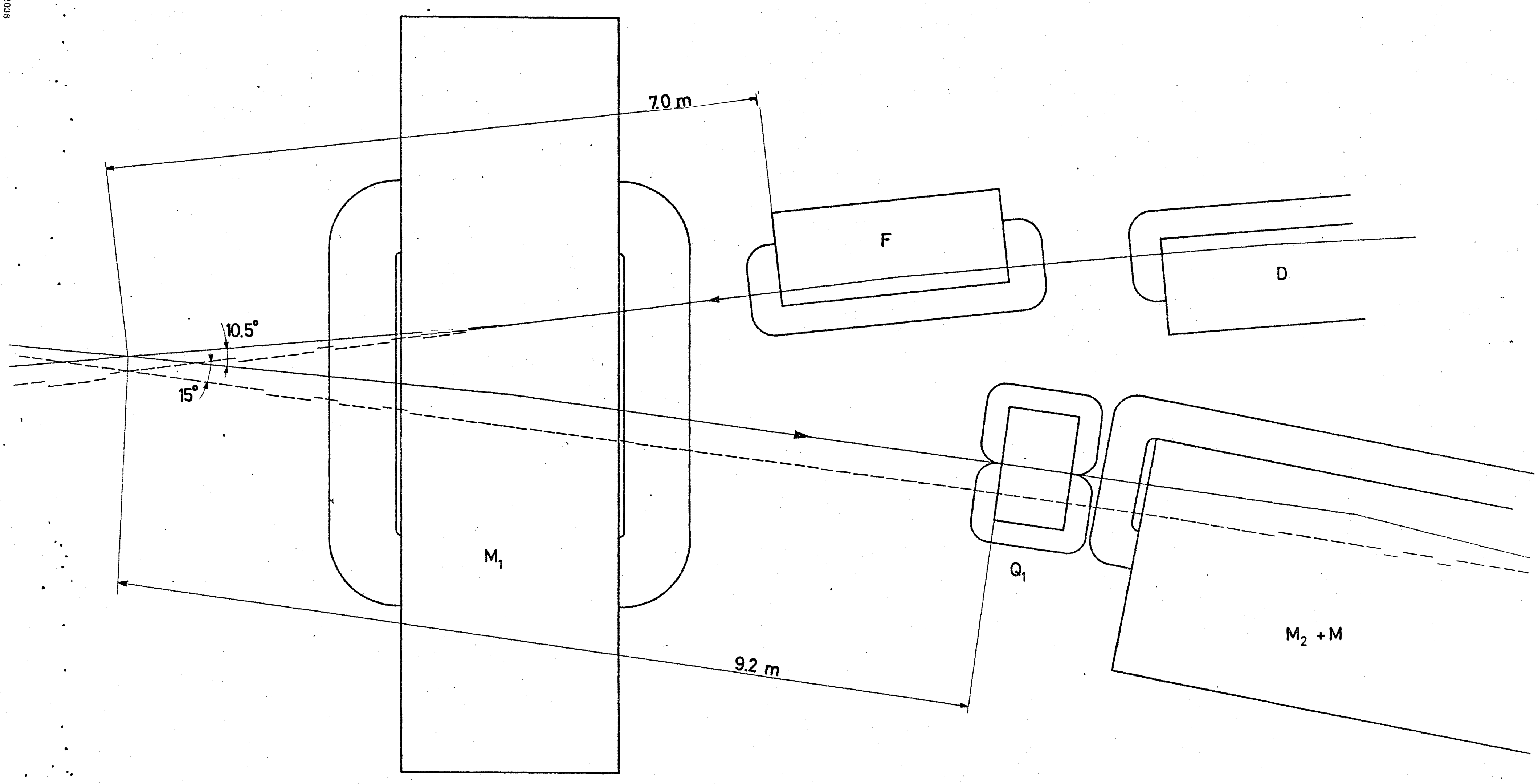

ALL PARAMETERS ARE THOSE AS GIVEN IN AR/INT SG/65-21

FIG. 16 STRUCTURE 1 WITH REDUCED CROSSING ANGLE AND SPECIAL MAGNET SECTION

STRUCTURE 1 WITH REDUCTED CROSSING ANGLE AND SPECIAL MAGNET SECTION

CERN ORGANISATION EUROPEENNE POUR LA RECHERCHE NUCLEAIRE - GENEVE

AR 203-270-1

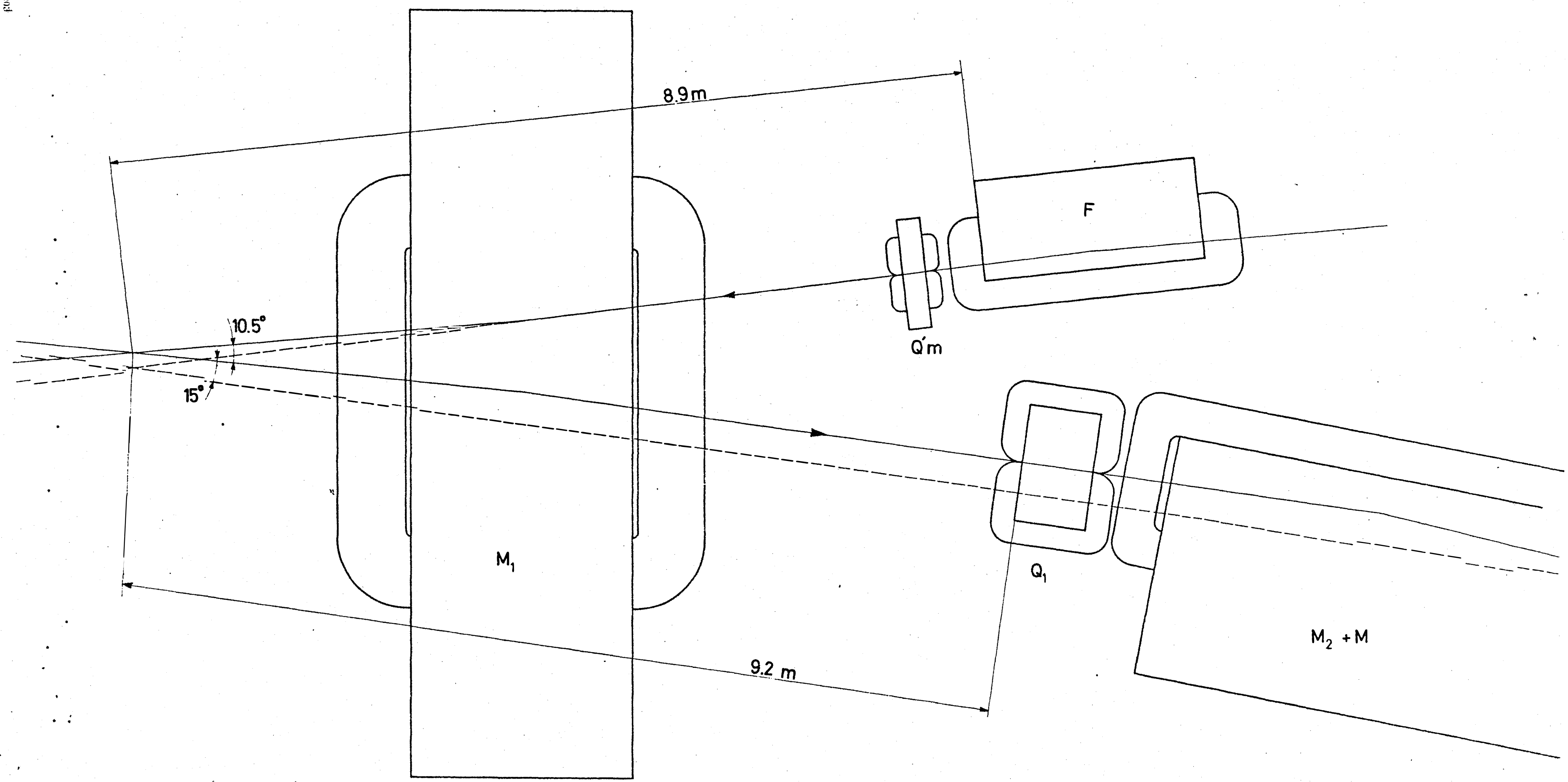

FIG. 17 STRUCTURE 2 WITH REDUCED CROSSING ANGLE AND SPECIAL MAGNET SECTION

ALL PARAMETERS ARE THOSE AS GIVEN IN AR/INT SG/65-21

STRUCTURE 2 WITH REDUCTED CROSSING ANGLE AND SPECIAL MAGNET SECTION

CERN ORGANISATION EUROPÉENNE POUR LA RECHERCHE NUCLÉAIRE - GENÈVE

AR 208-271-1

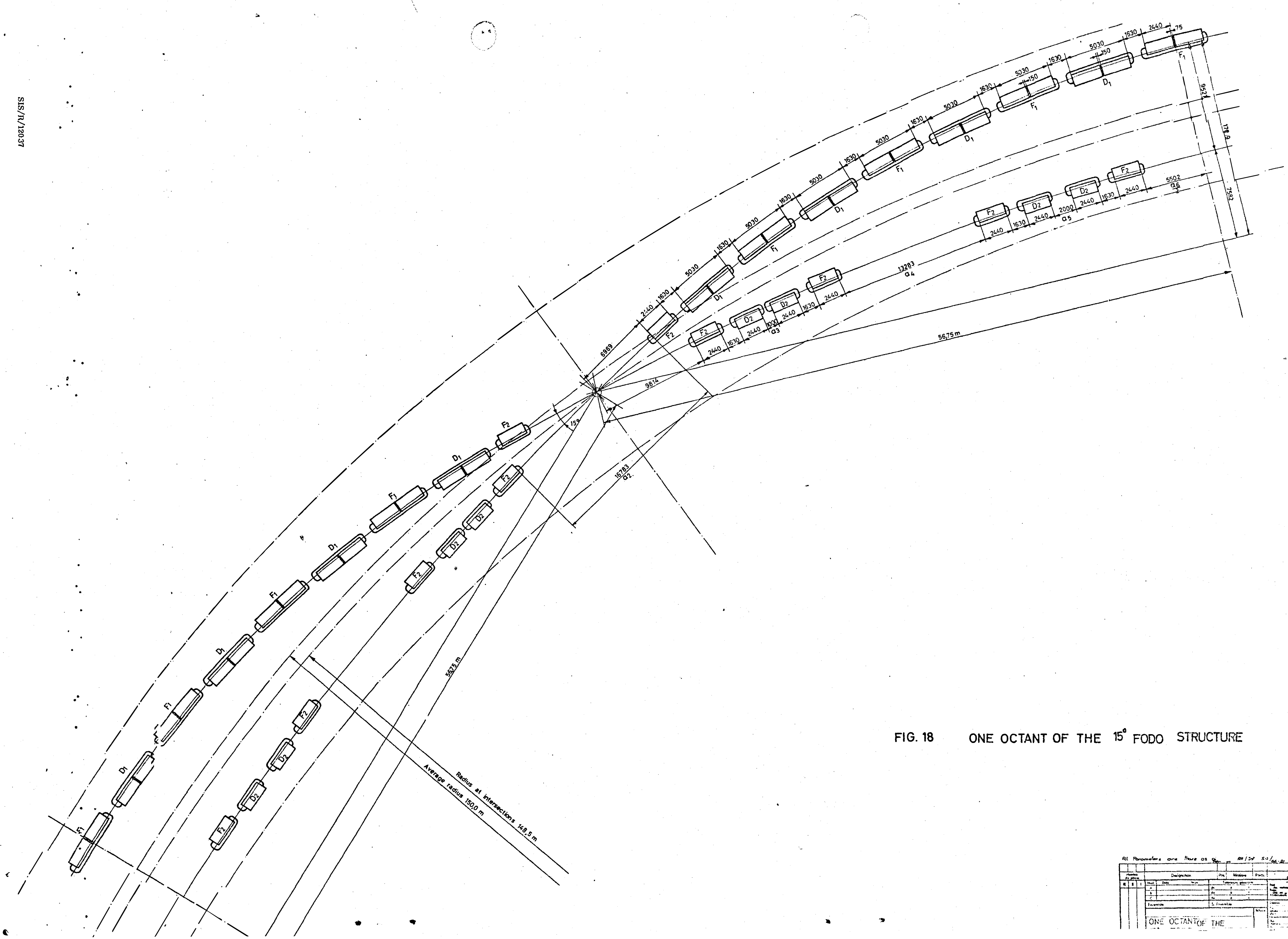

FIG. 18 ONE OCTANT OF THE 15° FODO STRUCTURE

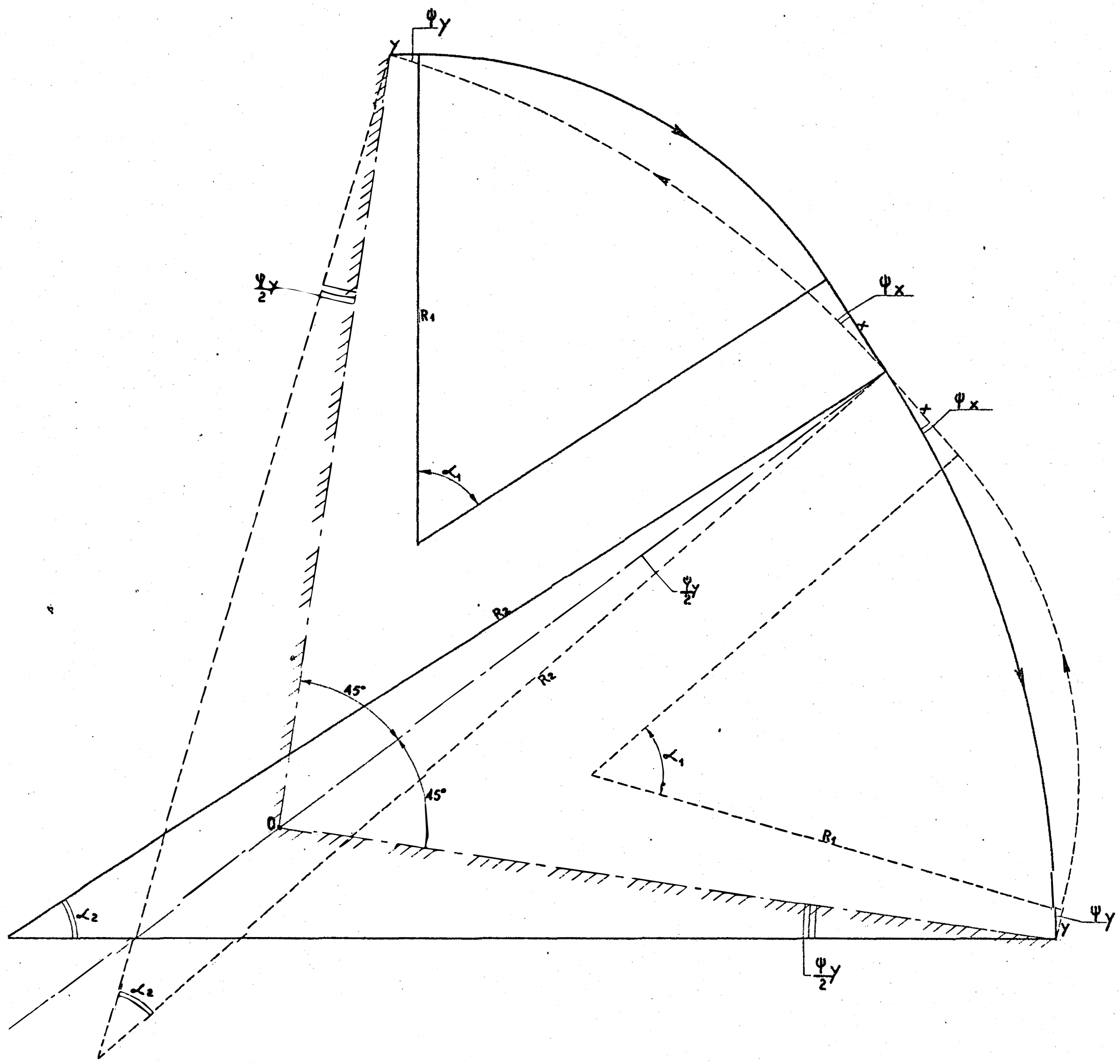

Fig.19 _ One of the 4 superperiods of a simple ISR structure with different crossing angles.

ALL PARAMETERS ARE THOSE AS GIVEN IN AR/INT SG/65_21

Nombre de pièces	Designation	Pos	Matière	Poids	Observations
III II I	Mod Date Nom	Tolerances générales			Etat des surfaces selon VSM 10320
	A	de			VSM
	B	de			VSM 10319
	C	de			

Ensemble | S. Ensemble | Echelle

Dessiné 25.11.65

Contrôlé

Vu

Remplace

Remplacé par

SCHEME OF ONE OF THE
4 SUPERPERIODS

Dossier N° | Dossier N° | Dossier N°

CERN ORGANISATION EUROPÉENNE POUR LA RECHERCHE NUCLÉAIRE - GENÈVE

AR 208-275-1.

SIS/R/12049

Fig. 20: One of the 4 superperiods of the case $N_1 = 7$ $N_2 = 5$ $\Psi_y = 10°45'$ $\Psi_x = 4°15'$ $R_{ave} \simeq 150$ m p=28 GeV/c

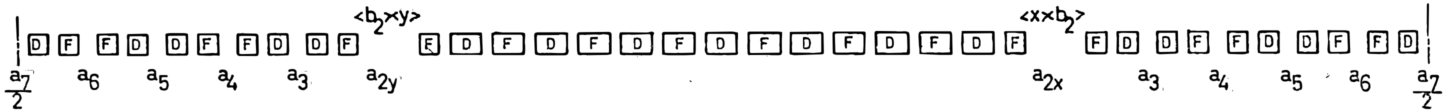

short magnets (steel)	= 2.44 m	$\frac{a_7}{2}$	=	2.23 m	a_3	=	2.00 m
long magnets (steel)	= 5.03 m	a_6	=	1.80 m	b_2	=	10.13 m
F D str. sections	= 1.63 m	a_5	=	2.00 m	y	=	6.00 m
		a_4	=	7.26 m	x	=	20.60 m

Fig. 21: One of the 4 superperiods of the case $N_1 = 7$ $N_2 = 4$ $\Psi_y = 16°$ $\Psi_x = 8\frac{6}{11}°$ $R_{ave} \simeq 150$ m p=25.8 GeV/c

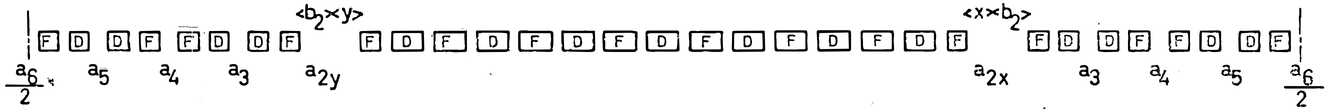

short magnets (steel)	= 2.47 m	x	=	21.01 m	a_4	=	13.13 m
long magnets (steel)	= 5.09 m	y	=	5.62 m	a_5	=	2.00 m
FD str. sections	= 1.63 m	b_2	=	9.00 m	a_6	=	10.28 m
		a_3	=	2.00 m			

ALL PARAMETERS ARE THOSE AS GIVEN IN AR/INT SG/65-21

Nombre de pièces	Désignation	Pos	Matière	Poids	Observations
III II I	Mod. / Date / Nom — A, B, C		Tolérances générales		Etat des surfaces selon VSM 10 320; Rugosité en µ VSM; Abréviations VSM 10 319
	Ensemble	S. Ensemble		Echelle	Dessiné 25-11-65; Contrôlé; Vu
	SCHEME OF ONE OF THE 4 SUPERPERIODS				Remplace; Remplacé par
Dossier No	CERN ORGANISATION EUROPEENNE POUR LA RECHERCHE NUCLEAIRE - GENEVE				AR-208-276-2-